JOURNAL OF PETROLOGY | VOLUME 43 | NUMBER 7 | PAGES 1177–1205 | 2002

Mantle Sources and the Highly Variable Role of Continental Lithosphere in Basalt Petrogenesis of the Kerguelen Plateau and Broken Ridge LIP: Results from ODP Leg 183

C. R. NEAL[1]*, J. J. MAHONEY[2] AND W. J. CHAZEY III[1]

[1]DEPARTMENT OF CIVIL ENGINEERING AND GEOLOGICAL SCIENCES, UNIVERSITY OF NOTRE DAME, NOTRE DAME, IN 46556, USA

[2]SCHOOL OF OCEAN AND EARTH SCIENCE AND TECHNOLOGY, UNIVERSITY OF HAWAII, HONOLULU, HI 96822, USA

RECEIVED JULY 13, 2001; REVISED TYPESCRIPT ACCEPTED JANUARY 31, 2002

Ocean Drilling Program (ODP) Leg 183 was designed to investigate the origin and evolution of the large igneous province composed of the Kerguelen Plateau and Broken Ridge. Of the eight sites drilled, basalt was recovered from seven, five on the plateau and two on Broken Ridge. We present results from four of these sites, 1136, 1138, 1141 and 1142. Although this large igneous province is interpreted as being derived from the Kerguelen mantle plume, the geochemical characteristics of basalt from some parts of the province indicate a role for continental lithosphere. The 118–119 Ma basalt flows recovered in the Southern Kerguelen Plateau (Site 1136) have a more subtle continental signature than shown by basalt at Leg 119 Site 738. A continental signature is absent in the 100–101 Ma tholeiitic basalts at Site 1138 in the Central Kerguelen Plateau (CKP); their age-corrected Nd–Sr–Pb isotopic values and incompatible element ratios are similar to those estimated for primitive mantle. These flows may represent a major mantle source in the Kerguelen starting-plume head. The 20 basalt units identified are a product of magma chamber replenishment, fractional crystallization, and resorption of crystallizing phases. The topmost unit, Unit 1, is a dacite that evolved from a basalt magma similar to those represented by Units 3–22; unlike the basalts the dacite magma was probably influenced by continental material. Middle Cretaceous (~95 Ma) lavas of Sites 1141 and 1142 on Broken Ridge (originally part of the CKP) are alkalic, with one exception (a tholeiite at the base of Site 1142). The alkalic lavas may represent a late-stage cap or carapace of relatively low-degree partial melts that overlies a thick tholeiitic lava pile. The tholeiite and pebbles from the top of a probable talus deposit (Unit 2) at Site 1142 have geochemical signatures consistent with a minor contribution from continental material. This signature is absent in the other units from these two sites, which have ocean-island-like incompatible element ratios and age-corrected isotopic characteristics similar (but not identical) to those proposed for the post-30 Ma Kerguelen plume. These alkalic basalts may be the purest representatives of the Cretaceous plume tail composition yet found.

KEY WORDS: *assimilation; basalt; large igneous province; mantle plume; Ocean Drilling Program*

INTRODUCTION

The Kerguelen Plateau and Broken Ridge constitute a large igneous province (LIP) in the southern Indian Ocean that originated after the ~132 Ma break-up of India and Australia (e.g. Kent *et al.*, 2002). The consensus view is that this LIP represents the volcanic outpouring from a starting-plume head that also produced magmatism in NE India (Rajmahal Traps; e.g. Mahoney *et al.*, 1983; Kent *et al.*, 1997, 2002), the Bunbury Basalt of

*Corresponding author. Telephone: 1-219-631-8328. Fax: 1-219-631-9236. E-mail: neal.1@nd.edu

southwestern Australia, and the Naturaliste Plateau off the southwestern coast of Australia (e.g. Storey *et al.*, 1992; Mahoney *et al.*, 1995; Frey *et al.*, 1996). Recent data from Leg 183 suggest several distinct stages of plateau building (Pringle & Duncan, 2000; Coffin *et al.*, 2002; Duncan, 2002). The Kerguelen Plateau is 200–600 km wide, extends for ~2300 km from 46°S to 64°S and contains the volcanic islands of Heard and McDonald, as well as the Kerguelen Archipelago (Fig. 1). If a plume model is accepted, these islands represent the most recent volcanic products of a long-lived Kerguelen plume tail that also produced the Ninetyeast Ridge (e.g. Frey *et al.*, 1991; Saunders *et al.*, 1991; Frey & Weis, 1995). Broken Ridge, located ~1800 km to the north, was separated from the main plateau by the opening of the Southeast Indian Ridge (SEIR) during the Early Tertiary (e.g. Tikku & Cande, 2000). Located approximately midway between the Kerguelen Archipelago and Broken Ridge on the SEIR are the relatively recent oceanic islands of Amsterdam and St. Paul (Fig. 1), the largest volcanoes of the Amsterdam–St. Paul hotspot.

The Kerguelen Plateau is broadly divided into southern, central, and northern domains (Fig. 1), each with a distinct crustal structure and thickness (e.g. Coffin *et al.*, 1990; Schaming & Rotstein, 1990; Frey *et al.*, 2000). The Southern Kerguelen Plateau (SKP) is composed of an igneous crust of ~22 km thickness that, on the basis of seismic velocities, may contain fragments of continental material, especially in the northern SKP (Operto & Charvis, 1995, 1996; Charvis *et al.*, 1997). The igneous crust of the Central Kerguelen Plateau (CKP) is between 19 and 21 km thick and does not contain the seismically reflective transition zone suggestive of continental material as seen in the SKP. The CKP includes the volcanic islands of Heard and McDonald, and, originally, Broken Ridge; Elan Bank extends westward from the CKP (Fig. 1). Seismically, the igneous basement of the Northern Kerguelen Plateau (NKP) is divided into an upper crust (8–9·5 km thick) and a lower crust (6–9·5 km thick) (Recq *et al.*, 1990, 1994; Charvis *et al.*, 1995).

Basement rocks of the Kerguelen Plateau have been sampled via dredging and drilling. Basalt was encountered at one drill site during Ocean Drilling Program (ODP) Leg 119 (Site 738) and four drill sites during ODP Leg 120 (Sites 747–750). Sites 738, 748, 749, and 750 are in the SKP, and Site 747 is in the CKP (Fig. 1). Basalt at Site 748 was an inter-sediment unit, whereas the cored basalt sequences at Sites 738, 747, 749, and 750 were more substantial and were considered to represent igneous basement (e.g. Barron *et al.*, 1989; Schlich *et al.*, 1989; Salters *et al.*, 1992; Storey *et al.*, 1992). The Ninetyeast Ridge was cored at four sites during Deep Sea Drilling Project (DSDP) Legs 22 (Sites 214 and 216) and 26 (Sites 253 and 254), and at three sites during ODP Leg 121 (Sites 756, 757, and 758) (see Frey *et al.*, 1977, 1991; Mahoney *et al.*, 1983; Baksi *et al.*, 1987; Davies *et al.*, 1989; Storey *et al.*, 1989, 1992; Saunders *et al.*, 1991; Frey & Weis, 1995, 1996). Dredged basalts from the Kerguelen Plateau, Naturaliste Plateau and Broken Ridge were studied by Davies *et al.* (1989), Weis *et al.* (1989), Storey *et al.* (1992), and Mahoney *et al.* (1995). The majority of basalts associated with the Kerguelen hotspot are tholeiitic or transitional between tholeiitic and alkalic (Coffin *et al.*, 2000) as defined by Macdonald & Katsura (1964).

Leg 183 of the Ocean Drilling Program drilled eight sites on the Kerguelen Plateau–Broken Ridge LIP (Coffin *et al.*, 2000). Seven of these sites reached igneous basement. Site 1135 (which cored only sediment) and Site 1136 were drilled in the SKP, Site 1137 in Elan Bank, Site 1138 in the CKP, Sites 1139 and 1140 in the NKP, and Sites 1141 and 1142 in Broken Ridge (CKP; see Fig. 1). The focus of this paper is the basement rocks recovered from Kerguelen Plateau Sites 1136 and 1138, and from Sites 1141 and 1142 on Broken Ridge.

General background

The influences of continental crust and/or lithospheric mantle have been documented in the continental portions of the Kerguelen LIP, the Rajmahal Traps (see Kent *et al.*, 1997, 2002) and Bunbury Basalt (Frey *et al.*, 1996). In the oceanic parts of the LIP, it has also has been recognized that a continental lithospheric mantle and/or crust signature is present in lavas of the SKP and CKP, Broken Ridge and the Naturaliste Plateau (e.g. Storey *et al.*, 1992; Mahoney *et al.*, 1995; Frey *et al.*, 2002), and that at least a small amount of continental lithospheric mantle is present in the NKP (Hassler & Shimizu, 1998). One of the major discoveries of Leg 183 was the presence of garnet–biotite gneiss cobbles in an inter-flow conglomerate from Site 1137 (Frey *et al.*, 2000; Nicolaysen *et al.*, 2001; Weis *et al.*, 2001; Ingle *et al.*, 2002*a*), which demonstrated the presence of Proterozoic continental crust in Elan Bank.

The longevity of the Kerguelen hotspot (which has been active for at least 120 Myr; Duncan, 2002) affords the opportunity to examine temporal compositional changes in hotspot-derived magmas. However, the highly variable influence and geochemical heterogeneity of continental lithospheric material complicate interpretation of geochemical data. Variations documented from pre-Leg 183 sampling were generally interpreted in terms of a plume-type model. Most workers have interpreted the lavas associated with the Kerguelen hotspot to reflect variable mixtures of a dominant Kerguelen plume

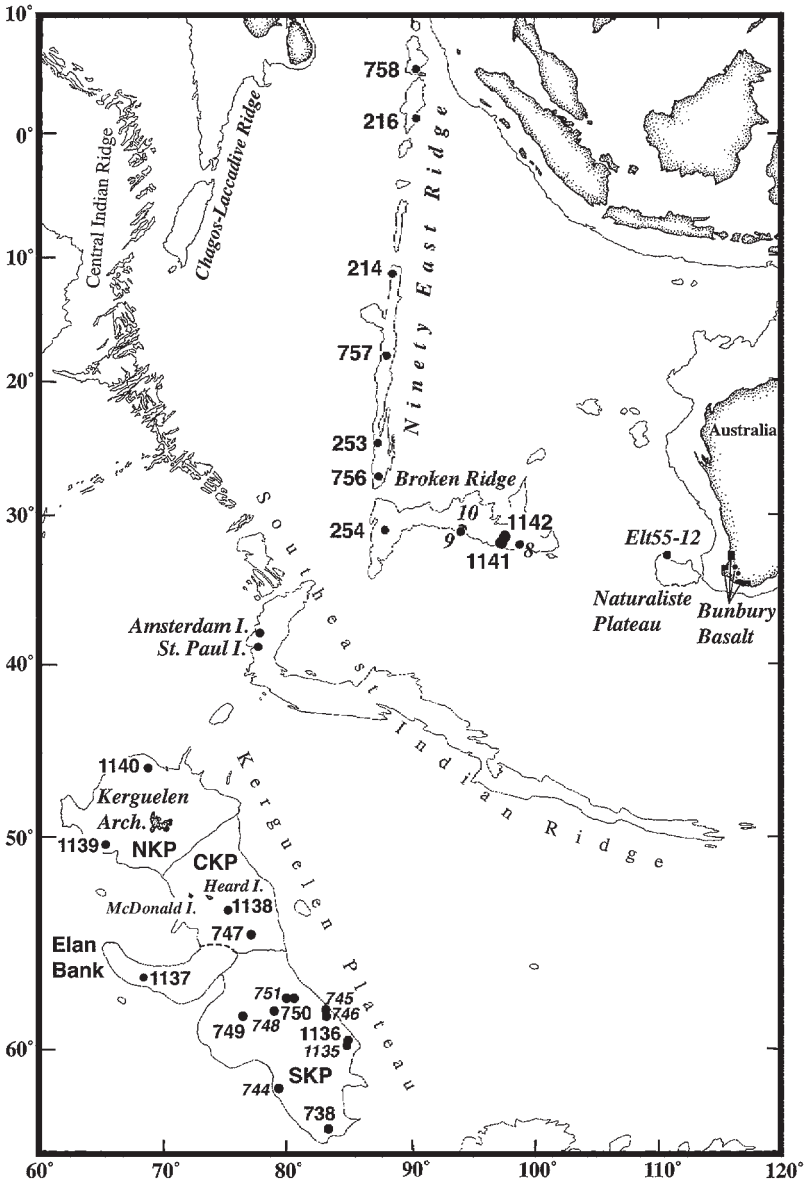

Fig. 1. Map of the Indian Ocean highlighting the features attributed to the Kerguelen hotspot and indicating the Southeast Indian Ridge. Both drill and dredge sample sites are numbered. On the Kerguelen Plateau, drill sites that did not reach basement are in italics. Adapted from Mahoney *et al.* (1995). NKP, Northern Kerguelen Plateau; CKP, Central Kerguelen Plateau; SKP, Southern Kerguelen Plateau.

component, a second, minor plume-type component (similar isotopically to recent products of the Amsterdam–St. Paul hotspot), plus small amounts of Indian mid-ocean ridge basalt (MORB)-type mantle (Storey *et al.*, 1988; Frey & Weis, 1995, 1996) and isotopically heterogeneous continental crustal and/or lithospheric mantle material (e.g. Weis *et al.*, 1989, 1991, 2001; Storey *et al.*, 1992; Mahoney *et al.*, 1995; Frey *et al.*, 2002).

SAMPLE PREPARATION AND ANALYSIS

The analytical strategy was to analyze, where possible, one sample for major and trace elements from each unit defined during shipboard description of the core (Coffin *et al.*, 2000). For the thicker units, at least two samples were analyzed. Unless otherwise stated, the samples

Table 1: Whole-rock composition (major and trace elements) of basalt samples from ODP Leg 183 Sites 1136, 1138, 1141, and 1142

Site:	1136	1136	1136	1136	1138	1138	1138	1138	1138	1138	1138	1138	1138	1138	1138	1138	1138	1138
Core:	16R	18R	18R	19R	74R	80R	80R	80R	81R	81R	82R	82R	83R	83R	84R	84R	85R	85R
Section:	2	3	6	2	1	1	2	5	2	4	1	5	6	6	1	5	1	2
Piece:	2A	2	6	9	4	13	1	1D	12	10	7B	2	3	5B	1E	9	16	7B
Unit:	1	2	2	3	1	3	4	5	6	7	8	9	10	11	12	13	14	15
wt %																		
SiO_2	50·5	51·5	50·8		*63·9*	49·2	48·7	48·9	48·7	48·0	47·3	48·2	47·8		48·8	48·6	48·0	48·6
TiO_2	1·75	1·68	1·65		*1·53*	1·92	2·17	2·16	2·05	2·04	2·19	2·12	2·26		2·32	2·18	2·56	2·62
Al_2O_3	15·9	15·2	14·5		*14·8*	16·5	16·0	15·9	15·5	15·5	14·6	14·2	14·5		14·6	14·4	13·8	13·0
Fe_2O_3	12·0	11·7	12·8		*9·33*	12·0	12·4	11·6	12·5	13·1	14·7	14·9	14·2		13·9	14·5	15·2	15·7
MnO	0·12	0·20	0·23		*0·04*	0·29	0·33	0·27	0·28	0·37	0·41	0·25	0·33		0·34	0·25	0·36	0·28
MgO	6·56	6·25	6·65		*0·25*	5·17	5·82	5·76	6·12	6·37	6·25	5·83	6·05		5·98	5·60	5·97	5·95
CaO	9·24	9·25	10·0		*3·58*	11·6	11·1	11·5	11·2	10·3	10·5	10·8	10·9		9·94	10·7	9·99	8·84
Na_2O	3·24	3·18	2·80		*3·53*	2·71	2·97	2·95	2·64	2·72	2·72	2·92	2·78		3·00	2·88	2·93	3·79
K_2O	0·32	0·32	0·27		*2·70*	0·19	0·22	0·21	0·76	0·86	0·43	0·20	0·33		0·50	0·21	0·39	0·69
P_2O_5	0·18	0·19	0·18	0·19	*0·58*	0·21	0·25	0·23	0·22	0·22	0·28	0·26	0·26		0·29	0·27	0·33	0·32
LOI	3·77	2·17	1·15		*1·69*	2·05	2·43	2·45	2·05	1·33	1·33	2·56	1·96		3·69	1·38	2·53	4·65
ppm																		
Li	3·7	8·7	5·9	9·1		6·2	6·2	7·0	7·0	8·9	12·0	5·3	6·2	10·6	7·6	6·8	16·8	14·3
Be	0·44	0·70	0·68	0·85	5·9	0·89	0·87	0·73	0·34	0·49	0·79	0·79	0·73	0·49	0·69	1·08	0·74	0·71
Sc	36·2	23·7	36·2	39·8	7·5	48·5	48·9	55·8	50·9	47·5	46·8	49·1	46·7	48·8	48·3	44·1	40·2	48·5
V	278	229	193	325	56·4	373	413	509	435	369	410	547	486	461	409	388	465	696
Cr	170	176	171	288	17·8	86·3	69·7	101	84·7	69·6	87·9	49·1	58·6	85·0	55·8	83·5	46·0	25·6
Co	46·0	41·6	48·9	22·0	9·64	50·9	40·1	50·7	49·2	47·2	42·3	56·9	46·2	52·9	48·7	50·1	46·5	54·8
Ni	65·3	59·3	59·8	34·7	12·4	57·3	49·9	67·0	56·4	57·6	50·1	50·9	46·4	49·7	43·8	42·5	35·1	38·1
Cu	48·7	128	118	150	41·7	139	73·9	157	133	189	139	204	150	179	180	167	202	243
Zn	112	122	111	82·0	114	130	107	147	135	133	120	162	131	170	148	129	162	190
Ga	19·6	21·8	19·4	22·0	1·83	20·2	19·5	21·8	20·8	20·3	19·7	20·3	19·8	22·9	21·7	20·1	22·8	20·0
Rb	4·1	2·7	4·0	20·9	60·1	2·0	2·1	1·3	9·2	11·2	5·4	6·5	3·0	2·9	5·4	1·0	4·9	7·9
Sr	229	240	232	257	187	234	245	254	205	205	210	205	199	212	245	209	210	324
Y	25·8	27·7	27·1	50·3	58·0	32·8	31·3	30·8	29·7	29·3	34·9	33·7	33·8	37·5	36·2	37·2	48·2	39·8
Zr	93·0	106	101	103	483	124	159	138	128	120	162	151	168	193	166	181	203	203
Nb	6·1	6·6	6·2	7·2	37·3	11·2	13·6	12·7	11·8	11·5	14·5	12·9	13·9	16·3	15·6	14·9	17·2	17·5
Mo	0·46	0·72	0·52	0·98	3·24	0·46	0·47	0·49	0·25	0·58	0·53	1·41	0·88	0·79	0·58	0·66	0·95	0·77
Cs	0·06	0·03	0·13	0·41	0·43	0·01	0·01	0·03	0·04	0·13	0·03	0·12	0·02	0·02	0·01	0·01	0·11	0·83
Ba	72·3	110	81·3	133	524	81·3	88·9	104	86·4	117	104	86·0	90·0	91·2	98·5	123	107	226

Site:	1136	1136	1136	1136	1138	1138	1138	1138	1138	1138	1138	1138	1138	1138	1138	1138	1138	1138
Core:	16R	18R	18R	19R	74R	80R	80R	80R	81R	81R	82R	82R	83R	83R	84R	84R	85R	85R
Section:	2	3	6	2	1	1	2	5	2	4	1	5	6	6	1	5	1	2
Piece:	2A	2	6	9	4	7	13	1	1D	12	10	7B	2	3	5B	1E	9	16
Unit:	1	2	2	3	1	3	4	5	6	7	8	9	10	11	12	13	14	15
La	7·51	8·79	8·52	11·1	48·1	11·0	12·2	11·2	11·3	11·2	12·9	13·9	14·4	14·1	14·3	15·1	16·9	17·2
Ce	17·2	21·5	20·2	30·3	97·6	25·9	28·7	26·8	27·1	27·5	32·2	29·9	31·6	32·9	36·2	36·6	42·4	36·6
Pr	2·61	3·08	2·96	4·74	13·1	3·83	4·23	3·91	3·91	3·85	4·70	4·49	5·00	4·77	5·28	4·98	6·22	5·73
Nd	12·6	14·2	13·8	24·0	53·7	17·1	18·9	17·7	17·4	17·5	21·5	19·9	22·4	22·0	23·0	21·7	26·4	25·0
Sm	3·64	4·12	4·03	7·91	12·8	4·49	4·87	4·61	4·58	4·70	5·51	5·08	5·63	5·67	5·80	5·77	6·65	6·17
Eu	1·45	1·58	1·44	2·35	3·37	1·58	1·74	1·66	1·66	1·71	1·88	1·76	1·95	2·04	1·99	1·76	2·07	2·13
Gd	4·55	5·44	5·07	8·38	11·8	5·33	5·53	5·41	5·35	5·46	6·29	5·92	6·43	6·88	6·78	6·66	7·99	7·38
Tb	0·80	0·86	0·88	1·41	1·90	0·92	0·93	0·89	0·93	0·96	1·08	1·00	1·10	1·12	1·15	1·10	1·31	1·22
Dy	4·91	5·56	5·21	8·63	11·1	5·73	5·68	5·62	5·97	5·90	6·80	6·25	6·98	6·67	7·30	6·99	8·46	7·54
Ho	0·98	1·07	1·02	1·77	2·17	1·26	1·16	1·15	1·22	1·25	1·44	1·34	1·49	1·42	1·56	1·48	1·78	1·59
Er	2·75	3·15	3·00	4·66	5·94	3·64	3·18	3·32	3·42	3·46	3·93	3·82	4·09	4·09	4·29	4·27	5·09	4·47
Tm	0·41	0·46	0·43	0·64	0·83	0·54	0·45	0·50	0·50	0·53	0·53	0·52	0·56	0·58	0·59	0·59	0·72	0·61
Yb	2·55	2·95	2·67	3·91	5·16	3·35	3·00	3·19	3·04	3·41	3·63	3·53	3·75	4·00	3·94	4·03	4·97	4·15
Lu	0·31	0·39	0·40	0·56	0·69	0·49	0·45	0·44	0·46	0·48	0·50	0·53	0·55	0·58	0·59	0·61	0·69	0·60
Hf	2·57	2·54	2·65	2·69	12·3	3·36	3·75	3·75	3·61	3·38	4·25	3·85	4·74	4·57	4·51	4·97	5·41	4·76
Ta	0·35	0·52	0·51	0·57	2·59	0·66	0·72	0·70	0·63	0·72	0·80	0·70	0·92	1·07	0·80	0·96	1·04	0·91
Pb	1·42	3·19	2·39	0·78	1·26	0·48	1·52	1·21	1·01	1·34	1·63	1·61	2·27	2·51	1·95	2·85	3·75	2·19
Th	0·93	0·91	1·02	1·10	6·48	1·02	1·35	1·20	0·98	1·24	1·50	1·32	1·80	1·814	1·69	1·59	1·95	1·83
U	0·08	0·19	0·22	0·33	1·24	0·18	0·15	0·14	0·15	0·24	0·27	0·25	0·35	0·39	0·31	0·40	0·48	0·38

Table 1: continued

Site:	1138	1138	1138	1138	1138	1138	1138	1141	1141	1141	1141	1141	1141	1141	1141	1141
Core:	86R	86R	86R	87R	88R	88R	89R	13R	17R	18R	19R	19R	21R	23R	24R	24R
Section:	1	3	4	2	1	2	3	1	CC	2	1	2	2	4	3	3
Piece:	2C	6	3	1	6B	10	1A			1	2	7	1D	2	2C	3B
Unit:	16	17	18	19	20	21	22	1	4	4	4	4	5	6	6	6
wt %																
SiO_2	47·4	47·6	46·6	48·4	46·6	47·4	47·6	48·2	47·2	47·8	47·1	47·2	49·7	46·9	47·5	47·7
TiO_2	2·91	2·72	2·83	2·90	2·95	2·95	3·05	2·85	3·52	3·13	2·81	2·77	3·14	2·76	2·75	2·74
Al_2O_3	13·9	13·8	14·6	14·2	14·3	13·5	13·5	19·7	18·3	16·9	15·8	15·9	17·8	16·7	16·7	16·3
Fe_2O_3	16·6	16·9	16·5	15·4	17·4	17·5	17·2	9·35	14·7	12·6	12·4	12·3	11·8	11·9	11·7	11·8
MnO	0·38	0·36	0·25	0·36	0·35	0·37	0·32	0·12	0·29	0·20	0·14	0·11	0·18	0·19	0·16	0·16
MgO	5·59	5·20	5·35	4·80	4·97	4·96	4·74	4·96	2·33	4·72	6·03	6·12	3·19	6·36	6·43	6·45
CaO	9·20	8·73	9·77	8·89	9·56	9·58	9·68	10·7	8·46	10·4	11·2	11·4	9·43	10·7	10·9	10·9
Na_2O	3·00	3·72	2·70	3·88	2·83	2·85	2·84	2·99	3·24	2·96	2·81	2·93	3·11	2·63	2·74	2·71
K_2O	0·47	0·23	0·60	0·36	0·33	0·28	0·25	0·93	0·63	0·62	0·74	0·74	0·91	0·80	0·79	0·76
P_2O_5	0·40	0·36	0·33	0·40	0·39	0·39	0·40	0·46	0·74	0·67	0·47	0·46	0·55	0·48	0·48	0·47
LOI	3·18	2·42	2·34	1·50	4·12	1·16	1·56		7·33	6·40			4·75	5·07		
ppm																
Li	21·9	24·5	24·0	14·8	13·8	15·4	12·4	5·5	0·4	2·4	4·0	2·4	4·0	1·9	2·6	2·7
Be	0·79	0·94	0·67	0·81	0·84	0·78	1·27	0·82	1·43	1·41	1·34	1·47	1·20	1·05	1·51	1·30
Sc	43·2	46·7	46·3	41·7	43·6	39·6	43·6	29·1	27·8	27·4	29·5	30·1	29·3	27·3	30·3	28·6
V	396	578	426	468	509	360	393	363	285	349	285	264	218	274	311	216
Cr	14·4	16·2	23·1	12·0	11·1	11·3	44·6	230	191	108	358	350	300	274	362	322
Co	46·7	51·2	50·4	44·2	52·4	52·6	51·8	35·7	60·3	50·9	57·0	35·4	58·9	47·8	53·9	51·6
Ni	28·9	32·6	31·6	25·5	26·7	25·6	28·2	95·2	166	138	198	145	208	179	200	195
Cu	190	209	197	214	204	184	238	195	216	336	214	256	194	213	238	202
Zn	178	188	189	168	168	153	175	155	148	178	132	117	126	100	130	119
Ga	23·0	20·9	21·4	16·8	21·5	21·0	23·0	17·4	22·3	22·5	19·3	20·5	18·5	20·5	18·0	18·4
Rb	17·7	2·8	9·2	3·9	2·9	2·6	3·1	13·0	3·3	10·8	6·2	8·7	6·7	7·4	8·6	8·7
Sr	216	211	206	357	221	214	231	458	591	537	493	477	523	422	461	443
Y	46·8	48·5	48·1	44·8	49·8	45·5	52·2	24·3	40·2	32·1	28·5	29·9	27·2	27·0	28·5	27·6
Zr	207	265	224	220	242	225	231	244	266	246	176	185	132	218	215	161
Nb	19·6	21·8	21·0	20·4	21·3	20·6	22·7	30·5	35·1	31·8	26·3	28·4	25·9	25·6	26·7	25·6
Mo	0·80	0·99	0·54	0·79	0·93	0·96	1·04	1·12	0·72	1·12	0·50	0·82	0·61	0·77	0·83	0·90
Cs	0·33	0·47	0·13	0·69	0·06	0·11	0·03	0·04	0·05	0·24	0·08	0·07	0·09	0·08	0·12	0·22
Ba	135	110	117	147	116	115	125	233	287	266	261	323	264	292	318	313

Site:	1138	1138	1138	1138	1138	1138	1138	1141	1141	1141	1141	1141	1141	1141	1141	1141
Core:	86R	86R	86R	87R	88R	88R	89R	13R	17R	18R	19R	19R	21R	23R	24R	24R
Section:	1	3	4	2	1	2	3	1	CC	2	1	2	2	4	3	3
Piece:	2C	6	3	1	6B	10	1A			1	2	7	1D	2	2C	3B
Unit:	16	17	18	19	20	21	22	1	4	4	4	4	5	6	6	6
La	22·2	19·3	23·1	20·7	22·2	20·7	23·2	23·5	30·0	26·4	20·3	22·8	20·5	20·2	21·8	21·1
Ce	53·2	42·4	52·3	45·4	47·5	51·5	55·2	56·4	71·9	61·6	51·9	57·2	52·7	46·2	55·0	52·9
Pr	7·27	6·47	7·02	6·90	7·41	7·40	7·67	7·34	10·5	9·55	7·32	8·18	7·48	7·50	7·87	7·43
Nd	30·7	28·8	29·8	29·4	31·8	30·5	32·1	31·0	43·0	39·8	30·6	33·4	31·9	31·5	33·2	31·3
Sm	7·75	7·30	7·55	7·61	8·25	7·85	8·37	6·73	9·75	8·84	7·04	7·85	7·01	7·22	7·36	7·09
Eu	2·51	2·35	2·53	2·40	2·56	2·32	2·60	2·07	3·11	2·72	2·37	2·41	2·19	2·27	2·38	2·26
Gd	8·92	8·40	8·79	8·73	9·37	8·89	9·53	4·79	9·78	8·90	7·40	7·80	7·12	7·08	7·28	7·31
Tb	1·51	1·40	1·45	1·47	1·56	1·51	1·53	0·78	1·40	1·28	0·96	1·06	1·00	1·03	0·99	0·99
Dy	9·60	8·55	8·92	9·11	9·53	9·35	9·80	4·97	7·75	7·06	5·75	6·37	5·71	5·74	6·26	5·87
Ho	2·03	1·83	1·90	1·95	2·05	1·98	2·11	0·92	1·40	1·27	1·09	1·15	1·06	1·11	1·16	1·11
Er	5·80	5·07	5·43	5·65	5·80	5·72	5·96	2·43	3·85	3·48	2·96	3·28	2·77	2·83	3·23	3·05
Tm	0·79	0·76	0·74	0·76	0·76	0·78	0·83	0·27	0·46	0·38	0·31	0·39	0·35	0·35	0·40	0·33
Yb	5·43	4·69	5·02	5·37	5·41	5·29	5·69	1·94	3·33	2·76	2·38	2·86	2·52	2·48	2·81	2·56
Lu	0·71	0·70	0·74	0·76	0·76	0·78	0·83	0·27	0·46	0·38	0·31	0·39	0·35	0·35	0·40	0·33
Hf	5·74	5·89	6·25	6·13	6·44	6·41	6·00	4·99	6·98	6·75	4·68	4·97	3·56	5·92	5·83	4·36
Ta	1·14	1·10	1·11	1·18	1·26	1·32	1·21	1·76	1·83	1·59	1·50	1·65	1·53	1·45	1·62	1·64
Pb	2·93	2·82	2·56	2·87	2·90	3·94	3·20	2·49	4·18	2·63	17·2	2·66	2·27	2·23	2·51	2·42
Th	2·43	2·44	2·22	2·63	2·59	2·37	2·39	1·60	1·10	1·21	1·02	1·24	1·06	1·27	1·22	1·20
U	0·44	0·50	0·41	0·52	0·52	0·50	0·54	0·44	0·18	0·22	0·24	0·18	0·15	0·25	0·32	0·22

Table 1: continued

Site:	1142	1142	1142	1142	1142	BHVO-1	BHVO-1	SD
Core:	2R	3R	3R	9R	10R	(Cert.)	Average	(ppm)
Section:	1	1	1	3	3		(n = 8)	
Piece:	2A	6	9	8	1			
Unit:	1	2	2	6	6			
wt %								
SiO_2	47·2	46·7	48·5	52·6	47·1			
TiO_2	2·78	2·77	2·81	2·19	2·81			
Al_2O_3	15·8	16·2	18·9	15·8	15·8			
Fe_2O_3	12·2	11·9	11·5	12·8	12·4			
MnO	0·18	0·16	0·10	0·34	0·14			
MgO	7·41	6·56	2·96	3·91	6·03			
CaO	10·6	11·3	8·80	8·11	11·2			
Na_2O	2·64	2·69	3·84	3·07	2·81			
K_2O	0·66	0·69	2·10	0·81	0·74			
P_2O_5	0·49	0·48	0·45	0·40	0·47	0·273	0·272*	0·001
LOI	3·18		2·30	1·28	5·92			
ppm								
Li	3·9	5·5	3·5	4·1	1·8	4·6	4·8	0·45
Be	1·59	1·77	1·49	1·07	0·77	1·10	0·98	0·13
Sc	30·2	25·1	30·0	30·4	33·5	31·8	32·5	1·20
V	386	260	269	346	404	317	317	38·7
Cr	405	151	396	50·3	20·7	289	302	41·6
Co	55·8	31·4	52·1	39·4	64·8	45·0	47·2	1·75
Ni	220	92·2	197	34·2	40·5	121	124	8·51
Cu	256	122	213	158	171	136	156	18·5
Zn	121	98·6	124	131	142	105	123	8·21
Ga	16·9	23·5	18·3	19·0	25·7	21·0	21·9	0·62
Rb	14·0	14·8	13·7	12·0	3·2	*11·0*	*9·8*	*0·55*
Sr	460	445	444	178	204	403	402	14·4
Y	28·5	33·2	29·1	36·1	36·9	*27·6*	*24·5*	*0·66*
Zr	223	324	212	182	193	179	169	7·3
Nb	26·8	30·9	26·8	14·3	15·6	19·0	19·1	0·72
Mo	0·95	0·41	0·97	0·59	0·57	1·02	1·03	0·10
Cs	0·16	0·17	0·15	0·14	0·08	0·13	0·08	0·03
Ba	260	515	285	344	313	139	132	5·47

Table 1: continued

Site:	1142	1142	1142	1142	1142	BHVO-1	BHVO-1	SD
Core:	2R	3R	3R	9R	10R	(Cert.)	Average	(ppm)
Section:	1	1	1	3	3		(n = 8)	
Piece:	2A	6	9	8	1			
La	21·3	47·2	22·0	20·1	21·5	15·8	15·5	0·55
Ce	55·4	91·3	55·4	45·0	44·5	39·0	39·5	1·71
Pr	7·78	12·4	7·86	5·68	6·12	5·70	5·61	0·19
Nd	33·3	48·6	35·3	23·9	24·1	25·2	24·7	1·11
Sm	7·59	9·56	7·56	6·05	5·53	6·20	6·36	0·34
Eu	2·35	2·84	2·37	1·89	2·05	2·06	2·07	0·08
Gd	7·47	9·52	7·68	6·86	6·61	6·40	6·51	0·31
Tb	1·02	1·35	1·11	1·05	1·04	0·96	0·98	0·08
Dy	5·86	6·98	6·03	7·14	6·31	5·20	5·40	0·17
Ho	1·10	1·36	1·15	1·48	1·27	0·99	0·99	0·04
Er	3·02	3·72	3·21	4·09	3·85	2·40	2·59	0·09
Tm	0·43	0·53	0·45	0·62	0·59	0·33	0·34	0·04
Yb	2·58	3·22	2·72	4·12	3·95	2·02	2·12	0·11
Lu	0·36	0·44	0·35	0·59	0·57	0·29	0·26	0·04
Hf	5·87	8·76	5·64	5·23	5·44	4·38	4·48	0·19
Ta	1·60	2·09	1·62	1·01	0·98	1·23	1·22	0·12
Pb	3·52	4·58	2·39	4·57	4·50	*2·051*	*2·08*	*0·27*
Th	1·15	6·11	1·23	3·20	3·64	*1·233*	*1·25*	*0·08*
U	0·32	0·28	0·24	0·58	0·56	0·42	0·41	0·05

Values in italics are taken from Coffin *et al.* (2000) and are shipboard XRF data from 1138-74R-1, 24–30 (Piece 4).
*P_2O_5 for BHVO-1 analyzed twice during the analysis of the Site 1136 Unit 3 sample. Certified values for BHVO-1 taken from Govindaraju (1989). (For BHVO-1 values in italics, see http://www.nd.edu/~icpmslab for details and explanation.)

analyzed were the least altered available and were chosen on the basis of the following criteria: (1) macroscopic observation; (2) thin section examination; (3) relative density and hardness. Trace element analyses (Table 1) were carried out at the University of Notre Dame (see http://www.nd.edu/~icpmslab). All surfaces that had been in contact with the drill bit were removed from samples with a water-cooled rock saw and the interior portions were cut into slabs of ~1 cm thickness. All sawn surfaces were then removed using a diamond wheel. The slabs were placed inside a plastic bag, sealed with duct tape, and struck with a duct-tape-covered hammer to reduce the sample to small enough chips (~1 cm) to pass through alumina jaw crushers. A portion of these chips was separated for isotope analysis at the University of Hawaii. The remaining chips were lightly leached in dilute (≤0·25 N) HCl in an ultrasonic bath and then rinsed several times in high-purity deionized (18 MΩ cm) water. After drying on a hot plate at ~50–75°C, the chips were examined under a binocular microscope and pieces containing veins or vesicles were removed. Remaining pieces were passed through the jaw crushers and then reduced to a powder in an alumina mill. We took great care to remove and avoid metallic contamination as certain trace elements (Pb, for instance) are significantly affected by such contamination. Splits of the powders were dissolved for trace element analysis by inductively coupled plasma mass spectrometry (ICP-MS) using the method described by Neal (2001). The ICP-MS analyses were conducted in six separate batches, resulting in 10 analyses of reference material BHVO-1. Reproducibility is generally better than 3–5% on the basis of duplicate analyses (Fig. 2). All the samples for which data are reported here were analyzed by ICP-MS at least twice. If the data suggested dissolution might have been incomplete (i.e. depletions in Zr and Hf on primitive mantle normalized plots), a $LiBO_2$ fusion method of sample preparation was employed. The latter preparation was conducted to ensure that Zr and Hf were not being retained in phases resistant to conventional inorganic acid attack (e.g. zircon). Major element compositions of the powders were analyzed by X-ray fluorescence (XRF) at the University of Massachusetts [see Rhodes (1996) and http://www.geo.umass.edu/xrf for details]. The *mg*-number [molar $Mg/(Mg + Fe^{2+})$] of the samples was calculated assuming that 15% of the total iron was Fe^{3+}. XRF data quality was monitored by analyzing reference material K-1919 and undertaking replicate analyses.

Isotopic ratios of Sr, Nd, and Pb (Table 2) were measured following preparation and measurement procedures outlined by Mahoney *et al.* (1998). As in our previous studies, isotope-dilution measurements of Rb, Sr, U, Th, Pb, Sm, and Nd abundances were made on the same splits of sample as used for isotopic analysis, to age-correct the isotopic ratios. Because these measurements were made on small (~2 mm) chips hand-picked from the bulk rock and subsequently subjected to acid-cleaning and, in many cases, to a multi-step acid-leaching procedure before dissolution, the elemental abundances derived by isotope dilution generally do not represent whole-rock values.

RESULTS

Site 1136

Basement recovered at Site 1136 was divided into three basaltic units by the shipboard scientific party (Coffin *et al.*, 2000). Only 53 cm of the highly altered rubbly top of Unit 3 was recovered and the sample had to be carefully hand-picked to obtain enough material suitable for trace element and isotopic work. All three Site 1136 units are plagioclase, clinopyroxene, ±olivine phyric.

Units 1 and 2 exhibit little variation in major element composition (e.g. *mg*-number = 0·55–0·56; TiO_2 = 1·65–1·75 wt %; Table 1), consistent with the shipboard XRF data (Coffin *et al.*, 2000). Except for their higher $(^{207}Pb/^{204}Pb)_t$, Units 1 and 2 are isotopically similar to the Site 1138 basalt units (Table 2, Figs 3 and 4); relative to their $\varepsilon_{Nd}(t)$ values, which are near zero, their $(^{206}Pb/^{204}Pb)_t$ and $(^{87}Sr/^{86}Sr)_t$ are slightly lower than found for the Kerguelen Archipelago, and $(^{206}Pb/^{204}Pb)_t$ is much lower than for Heard Island at similar ε_{Nd}.

Trace element and isotope data demonstrate that Unit 3 is distinct (Tables 1 and 2; Figs 3–5), with higher REE (rare earth element) and Y abundances, a depletion in the LREE (light REE) relative to the heavy REE (HREE), markedly higher $\varepsilon_{Nd}(t)$, and more radiogenic $(^{208}Pb/^{204}Pb)_t$ and $(^{87}Sr/^{86}Sr)_t$ than Units 1 and 2. The sample is the most altered of any that we analyzed in this study, as indicated by the marked elevation of normalized U, Ba and, particularly, Rb abundances relative to Th and Nb (Fig. 5a). In contrast to Units 1 and 2, Unit 3 is not anomalously enriched in Pb. High field strength element abundances are broadly similar for all three units, although Units 2 and 3 have primitive mantle normalized (Sun & McDonough, 1989) Nb/Ta ratios $[(Nb/Ta)_{PM}] < 1$; these signatures, and the marked depletion in Zr and Hf relative to the REE in the Unit 3 pattern, have been replicated through two different dissolutions of the rock powder and one $LiBO_2$ fusion. The age-corrected $\varepsilon_{Nd}(t)$ value (+5·1) of the Unit 3 lava is by far the highest of any among our Leg 183 samples and similar to the highest values measured for basalts from Leg 120 Sites 749 and 750 (Storey *et al.*, 1992; Frey *et al.*, 2002). Its $(^{87}Sr/^{86}Sr)_t$ (0·70502) is similar to values for Site 750, which are higher for their $\varepsilon_{Nd}(t)$ than seen for any other Kerguelen Plateau, Broken Ridge, Kerguelen Archipelago, or Heard or McDonald Island lavas. However,

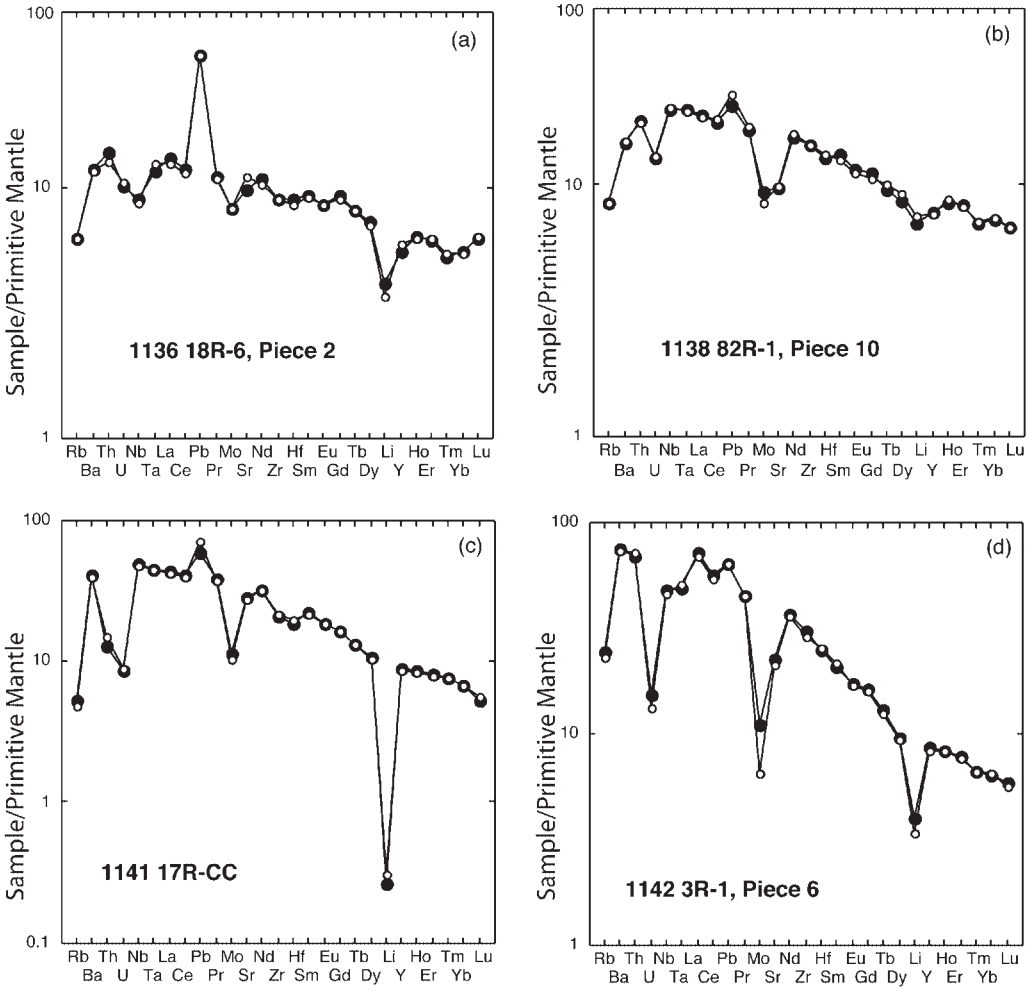

Fig. 2. Primitive mantle normalized incompatible element profiles of duplicate ICP-MS analyses of ODP Leg 183 basalts from Sites 1136, 1138, 1141, and 1142. Primitive mantle values are from Sun & McDonough (1989).

we caution that the high degree of alteration of the rock recovered from Unit 3 could mean that a significant amount of alteration-related Sr could have survived aggressive acid-leaching and that the $(^{87}Sr/^{86}Sr)_t$ value in Table 2 thus could be higher than the magmatic value.

Site 1138

Basement recovered at Site 1138 was divided into 22 igneous units (Coffin *et al.*, 2000), including cobbles of aphyric to sparsely feldspar-phyric dacite (Unit 1; shipboard XRF major element data for this unit are presented in Table 1) and an interbedded lithic breccia–volcanic ash sequence of 24·3 m thickness (Unit 2) containing completely altered clasts of highly plagioclase–clinopyroxene-phyric basalt. Units 3–22 represent a sequence of tholeiitic basalt flows, some with oxidized flow tops, interpreted as being erupted subaerially (Coffin *et al.*, 2000; Keszthelyi, in preparation). The basalts are aphyric to sparsely plagioclase–clinopyroxene-phyric, with plagioclase present either as solitary crystals or as glomerocrysts. Olivine microphenocrysts (partially to completely replaced by clay) are present in Units 5–16 and 19 and minor titanomagnetite phenocrysts are present throughout.

The Site 1138 basalt data appear to be consistent with a sequence of eruptions from a magma chamber undergoing progressive fractional crystallization, except there is a systematic increase in *mg*-number from the bottom to the top of the lava sequence (Fig. 6), the stratigraphic opposite of what would be expected. The compatible elements Sc, Cr, and Ni correlate positively with *mg*-number, as do CaO and Al_2O_3. MgO (4·7–6·4 wt%), Cr (11·1–101 ppm), and Ni (25·5–67·0 ppm) abundances are low in all of these basalts; thus, all are differentiated well beyond any plausible primary magma

Table 2: Isotopic ratios and isotope-dilution concentration data

Sample		$^{143}Nd/^{144}Nd$	$^{87}Sr/^{86}Sr$	$^{206}Pb/^{204}Pb$	$^{207}Pb/^{204}Pb$	$^{208}Pb/^{204}Pb$	Nd	Sm	Sr	Rb	Pb	U	Th	$\varepsilon_{Nd}(t)$	$(^{87}Sr/^{86}Sr)_t$	$(^{206}Pb/^{204}Pb)_t$	$(^{207}Pb/^{204}Pb)_t$	$(^{208}Pb/^{204}Pb)_t$
Kerguelen Plateau, Site 1136: t= *120 Myr*																		
16-2 pc 2 Unit 1	UL	0·512673	0·70466	17·955	15·565	38·373	13·32	4·058	226·9	2·56	1·467	0·1248	0·866	+0·8	0·70461	17·854	15·560	38·144
	L			17·906	15·563	38·229					0·3864	0·0104	0·0176			17·874	15·561	38·211
18-6 pc 2 Unit 2	UL																	
	L	0·512704	0·70469	17·911	15·580	38·369	3·518	1·425	162·4	1·78	0·5126	0·0322	0·153	+0·5	0·70463	17·837	15·576	38·253
19-2 pc 9 Unit 3	L	0·512887	0·70543	18·181	15·586	38·865	3·478	1·017	340·9	27·9	0·5479	0·0869	0·343	+5·1	0·70502	17·991	15·577	38·620
Kerguelen Plateau, Site 1138: t= *102 Myr*																		
74-1 pc 4 Unit 1	L	0·512608	0·70680	17·966	15·478	38·305	11·83	2·673	179·5	12·8	5·807	1·108	4·45	+0·2	0·70650	17·775	15·469	38·053
80-5 pc 1 Unit 5	UL	0·512632	0·70478	18·063	15·501	38·383	17·29	4·537	237·7	1·04	1·567	0·1958	1·07	+0·3	0·70477	17·937	15·495	38·158
	L	0·512684	0·70467	17·994	15·498	38·203	2·894	1·053	245·2	0·574	0·6038	0·0545	0·043	+0·6	0·70466	17·904	15·494	38·179
84-5 pc 3 Unit 13	UL	0·512652	0·70480	18·150	15·497	38·404	21·23	5·415	203·7	8·49	1·951	0·3548	1·50	+0·8	0·70462	17·967	15·488	38·150
	L	0·512699	0·70478	18·124	15·500	38·377	7·178	2·578	179·0	7·52	1·064	0·1472	0·629	+0·9	0·70460	17·985	15·493	38·182
86-3 pc 2 Unit 17	UL	0·512634	0·70472	18·157	15·512	38·482	26·39	6·707	159·4	3·14	2·232	0·4923	2·23	+0·4	0·70464	17·935	15·501	38·151
	L	0·512686	0·70469	18·117	15·493	38·417	5·583	2·089	180·9	1·97	0·5069	0·1025	0·195	+0·5	0·70464	17·913	15·483	38·290
89-3 pc 1 Unit 22	UL	0·512638	0·70471	18·109	15·499	38·390	32·20	8·117	217·9	2·01	3·216	0·5679	2·48	+0·5	0·70467	17·931	15·490	38·136
	L	0·512698	0·70465	18·060	15·495	38·342	5·222	2·014	221·6	0·403	0·3592	0·0281	0·057	+0·7	0·70464	17·981	15·491	38·290
Broken Ridge, Site 1141: t= *95 Myr*																		
13-1 pc 1 Unit 1	L	0·512656	0·70545	18·092	15·598	38·732	4·739	1·443	463·4	14·4	1·080	0·0453	0·151	+0·5	0·70533	17·989	15·593	38·689
18-2 pc 1 Unit 4	L	0·512646	0·70563	18·100	15·615	38·880	11·09	2·859	573·2	10·7	1·998	0·1623	0·712	+0·6	0·70556	17·997	15·610	38·770
2nd run, L				18·101	15·616	38·873										17·998	15·611	38·763
23-4 pc 2 Unit 6	UL	0·512629	0·70551	18·125	15·604	38·800	33·51	7·521	457·5	8·86	2·386	0·2847	1·32	+0·5	0·70543	18·022	15·599	38·629
	L	0·512650	0·70549	18·100	15·592	38·716	8·568	2·427	497·2	9·43	2·494	0·2597	0·938	+0·5	0·70541	17·997	15·587	38·600
2nd split, L				18·100	15·591	38·709					2·495					17·997	15·586	38·593
Broken Ridge, Site 1142: t= *95 Myr*																		
2-1 pc 2 Unit 1	UL	0·512620	0·70548	18·104	15·596	38·780	33·54	7·538	439·0	5·62	2·307	0·2422	1·32	+0·3	0·70543	18·001	15·591	38·603
	L	0·512647	0·70545	18·085	15·590	38·722	8·143	2·448	482·3	5·17	1·125	0·0812	0·033	+0·3	0·70541	18·017	15·587	38·631
9-3 pc 8 Unit 6	L	0·512675	0·70591	17·998	15·625	38·970	7·505	2·392	163·5	15·2	4·104	0·3952	2·03	+0·7	0·70555	17·895	15·620	38·817

L, strongly acid-leached powder; UL, unleached, but rock chips hand-picked and acid-cleaned. Isotope data are reported relative to values of $^{87}Sr/^{86}Sr = 0·71024$ for NBS 987 Sr, $^{143}Nd/^{144}Nd = 0·511850$ for La Jolla Nd, and the Pb isotope values of Todt *et al.* (1996) for NBS 981 Pb. The total range measured for NBS 987 Sr over a 2 year period was $\pm 0·00002$; for La Jolla Nd it was $\pm 0·000011$ (0·2 ε_{Nd} units); for NBS 981 Pb it was $\pm 0·011$ for $^{206}Pb/^{204}Pb$, $\pm 0·010$ for $^{207}Pb/^{204}Pb$, and $\pm 0·031$ for $^{208}Pb/^{204}Pb$. Within-run errors on the isotopic data above are less than the external uncertainties on these standards. Total procedural blanks are <35 pg for Pb, <46 pg for Sr, <15 pg for Nd. The isotope-dilution abundance data are in ppm; uncertainties are 0·2% for Sm and Nd, 0·4% for Sr, and 0·5% for Pb, 1% for Rb and U, and 2% for Th. Ages used for age corrections are from M. S. Pringle (personal communication, 2001). It should be noted that $\varepsilon_{Nd} = 0$ today corresponds to $^{143}Nd/^{144}Nd = 0·51264$; for Bulk Earth $^{147}Sm/^{144}Nd = 0·1967$, $\varepsilon_{Nd}(t) = 0$ at 95, 102, and 120 Ma, respectively, corresponds to $(^{143}Nd/^{144}Nd)_t = 0·512518$, 0·512509, and 0·512486.

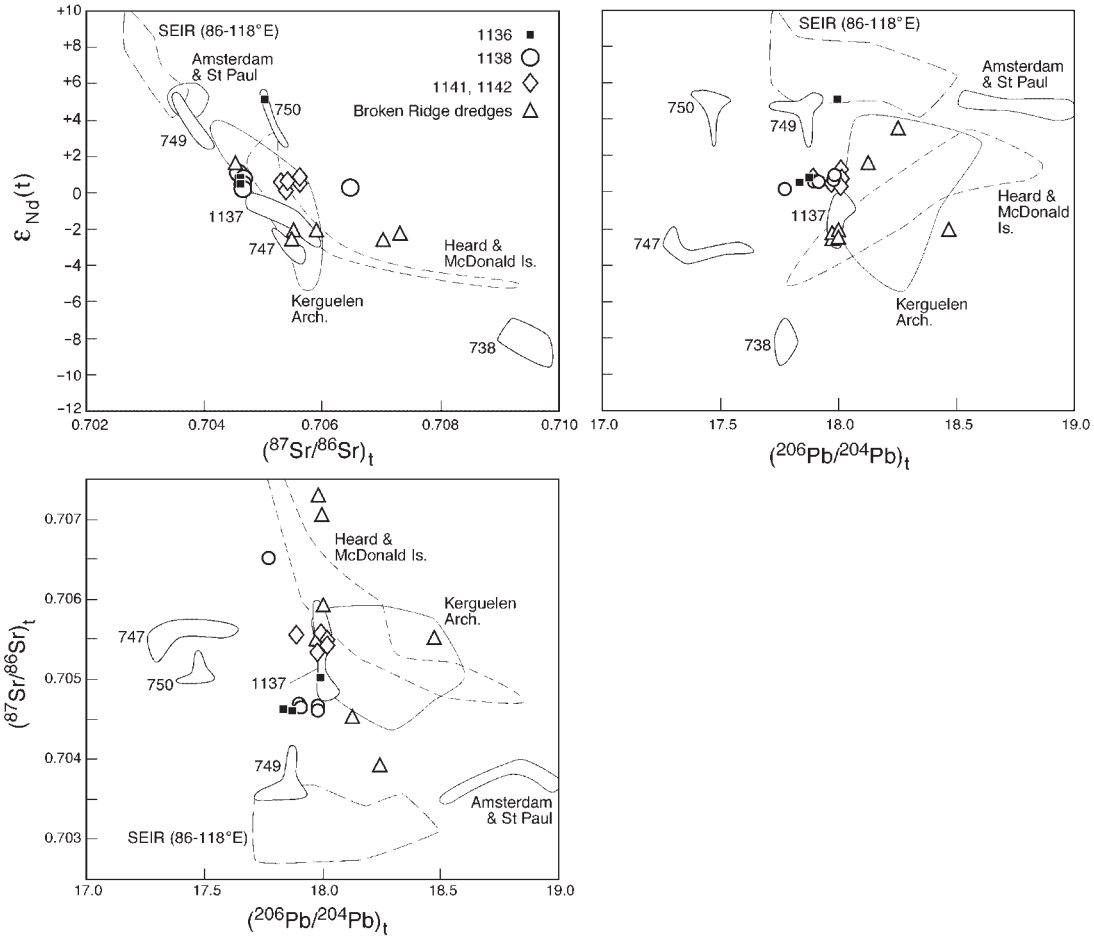

Fig. 3. Age-corrected isotopic ratios of basement rocks from Sites 1136, 1138, 1141, and 1142 (see Table 2). Age-corrected fields for Sites 747, 749, and 750 lavas (Frey *et al.*, 2002), and a non-age-corrected field for Site 1137 (Ingle *et al.*, 2002*b*) are shown. Data for dredged samples from Broken Ridge (age-corrected Nd and Sr isotopic ratios, present-day Pb isotopic ratios) and field for Site 738 (present-day values) are from Mahoney *et al.* (1995). Fields for the Kerguelen Archipelago (Dosso *et al.*, 1979; Dosso & Rama Murthy, 1980; Storey *et al.*, 1988; Gautier *et al.*, 1990; Weis *et al.*, 1993, 1998; Yang *et al.*, 1998), Heard and McDonald Islands (Storey *et al.*, 1988; Barling *et al.*, 1994), Amsterdam and St. Paul Islands (Hamelin *et al.*, 1986; Michard *et al.*, 1986; Dosso *et al.*, 1988; Salters & White, 1998; W. M. White, unpublished data, 2000), and the Southeast Indian Ridge (SEIR) between 86°E and 118°E (Mahoney *et al.*, 2002) are included for reference.

compositions. The dacite has low MgO, Fe_2O_3, and CaO, and relatively high alkali and P_2O_5 contents relative to the basalts (Table 1).

Incompatible element abundances, including TiO_2 and P_2O_5, are negatively correlated with *mg*-number (Fig. 6). Incompatible element ratios Nb/Ta, La/Nb, and Th/Ta, normalized to estimated primitive mantle values (Sun & McDonough, 1989), give an average value of 1·0 $\pm$ 0·1 for the entire suite of 20 basalt units. On primitive mantle normalized and chondrite-normalized plots, the basalt data form subparallel patterns (Fig. 7) with a pronounced depletion in Sr and P, and a slight depletion at Ce and Y. The dacite has a similar pattern to the basalts for elements to the right of Sr, except for a marked depletion in Ti (Fig. 7a) and greater LREE enrichment (Fig. 7b). In contrast to the basalts, however, it exhibits an enrichment of La and Th over Nb and Ta (Fig. 7a).

The effect of secondary processes on the Site 1138 basalt units is highlighted by the negative Ce anomaly in many of the samples (Fig. 7b). This is unlikely to be a primary igneous feature (e.g. Neal & Taylor, 1989). Rather, it suggests that relatively oxidizing conditions prevailed during alteration, promoting the oxidation of Ce^{3+} to Ce^{4+} and preferential removal of Ce. In addition, the highly variable Ba/Rb ratios (7·6–118·8) are distinct from the average ocean island basalt (OIB) and MORB value of $\sim$11 (e.g. Hofmann & White, 1983; Sun & McDonough, 1989) and are probably a result of alteration.

Age-corrected Sr, Nd, and Pb isotope ratios for the basalts exhibit very little variation throughout the sequence and the data generally plot close to the field

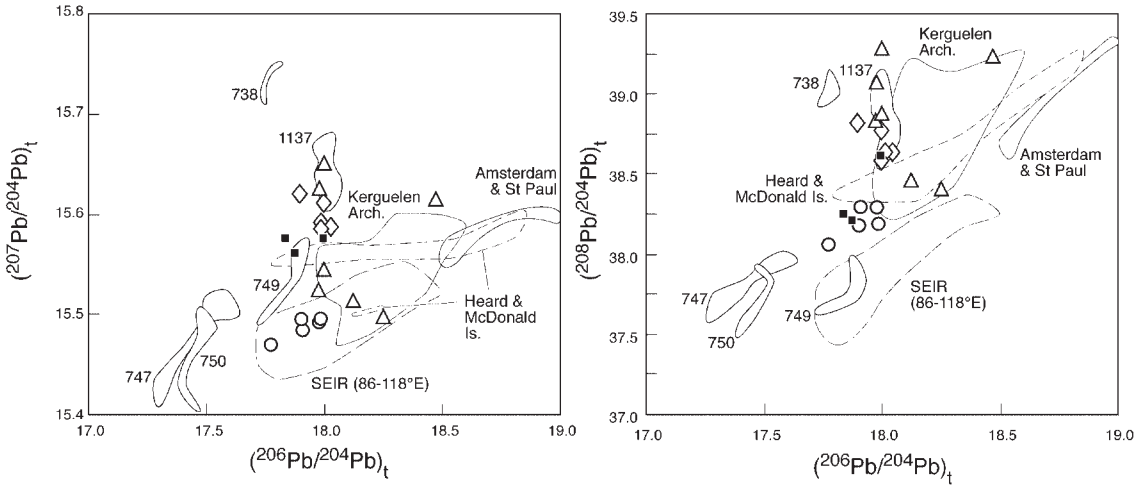

Fig. 4. Lead isotopic ratios of basement rocks from Sites 1136, 1138, 1141, and 1142 (see Table 2). Age-corrected fields for Sites 747, 749, and 750 lavas (Frey *et al.*, 2002), and a non-age-corrected field for Site 1137 (Ingle *et al.*, 2002*b*) are shown. Data for dredged samples from Broken Ridge (open diamonds, present-day values) and field for Site 738 (present-day values) are from Mahoney *et al.* (1995). Other data sources and symbols are as in Fig. 3.

defined by Kerguelen Archipelago lavas (Figs 3 and 4), at slightly lower $^{206}Pb/^{204}Pb$. The one isotopically distinctive igneous unit at Site 1138 is the Unit 1 dacite, which has significantly higher $(^{87}Sr/^{86}Sr)_t$ (0·7065) and slightly lower Pb isotope ratios than the basalts, but similar $\varepsilon_{Nd}(t)$ (+0·2).

Sites 1141 and 1142

Despite a distance of only ~800 m between Sites 1141 and 1142, the basement sections recovered differ considerably. Seismic reflection data revealed that the lower portion of the sedimentary sequence (i.e. below an erosional unconformity associated with the Eocene breakup of Broken Ridge and the CKP) dips northward in this area, suggesting that the basement section encountered at Site 1142 may be stratigraphically deeper than that at Site 1141 (Coffin *et al.*, 2000). Indeed, shipboard elemental data suggested that Unit 6 at Site 1141 and Unit 1 at Site 1142 may be the same unit (Coffin *et al.*, 2000; Tables 1 and 2). Our results support this interpretation.

Each Broken Ridge site contains six basement units, all of which were erupted subaerially, with the possible exception of Unit 6 at Site 1142 (Coffin *et al.*, 2000). At Site 1141, Unit 1 is composed of three small pieces (2–3 cm) of moderately altered plagioclase–clinopyroxene–olivine microgabbro. Units 2–6 are aphyric to plagioclase- and/or olivine-phyric basalts. Basement units at Site 1142 are basalt to basaltic andesite, and are aphyric to olivine and/or plagioclase phyric except for Unit 2, a probable talus deposit that contains pebbles of highly altered quartz-phyric lavas in a volcanic breccia.

All of the Broken Ridge basaltic units are alkalic, except for Unit 6 at Site 1142 (Coffin *et al.*, 2000). The lavas are relatively fractionated, containing 3·0–7·4 wt % MgO (Table 1). Both the alkalic and tholeiitic basalts are LREE enriched, although the former exhibit more extreme enrichments (Fig. 8a). Two samples analyzed from different pebbles of the Site 1142 talus deposit (Unit 2) have distinct major and trace element compositions (Table 1). Generally, the basalts from Sites 1141 and 1142 are enriched in the incompatible elements relative to the central Broken Ridge dredge samples (which were all tholeiitic basalts) reported by Mahoney *et al.* (1995) (see Fig. 8). The eastern Broken Ridge dredge samples are similar to the tholeiite at Site 1142 (Unit 6; Fig. 8b). The alkalic basalts exhibit a slight depletion in Y and several also show depletions of Zr and Hf relative to Nd and Sm (Fig. 8a). In addition, Nb and Ta are enriched relative to La and Th, and all exhibit a marked depletion in Th (Fig. 8a) as well as U. The Site 1142 tholeiitic basalt is distinguished from the alkalic basalts by the following features: (1) La and Th are enriched relative to Nb and Ta; (2) $(Sr/Nd)_{PM}$ <1 and Eu/Eu* (where Eu* is the estimated Eu abundance assuming a smooth REE profile) is slightly less than unity. The small sample of the Site 1141 microgabbro (Unit 1) is distinct from the basalts only in that it has a suprachondritic Zr/Hf ratio; this has been replicated in a separate analysis, but its origin is enigmatic.

Isotopically, the microgabbro is equivalent to the alkalic basalts from both sites, but the tholeiitic basalt

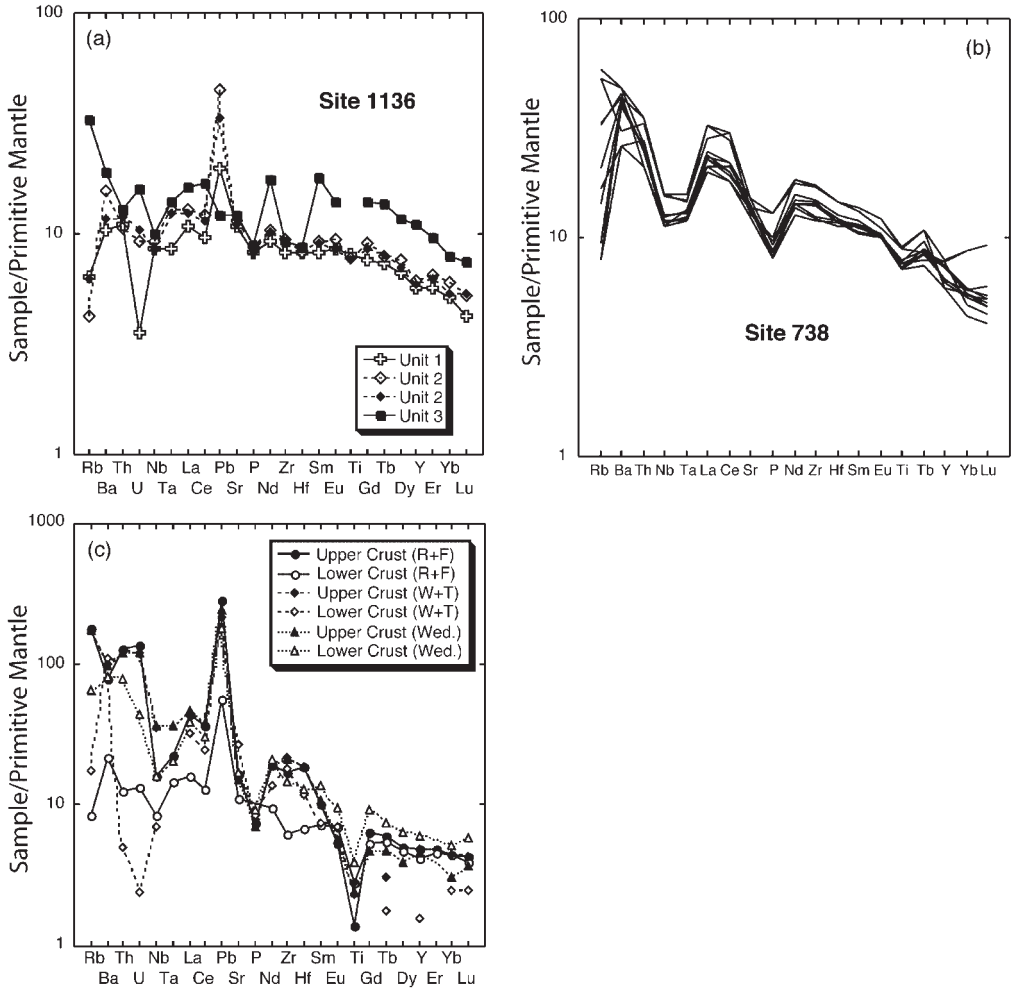

Fig. 5. Primitive mantle normalized incompatible element profiles of basalts from the Southern Kerguelen Plateau, as well as estimates of average upper and lower continental crust. In (c), 'R + F' refers to Rudnick & Fountain (1995), 'W + T' refers to Weaver & Tarney (1984), and 'Wed.' refers to Wedepohl (1995). Data for basalts from Site 738 were taken from Mehl *et al.* (1991) and Mahoney *et al.* (1995). It should be noted that (b) does not contain data for all of the elements listed in (a) and (c).

of Unit 6 at Site 1142 is distinct in that it has a slightly lower $(^{206}Pb/^{204}Pb)_t$ ratio (Figs 3 and 4 and Table 2). In terms of Sr and Nd isotopes, the Site 1141 and 1142 samples are nearly indistinguishable (Table 2), and plot roughly in the middle of the range defined by the dredged basalts from the central and eastern Broken Ridge. Their $\varepsilon_{Nd}(t)$ values are slightly positive, similar to those of the Site 1138 basalts and the upper two lava units at Site 1136; however, their $(^{87}Sr/^{86}Sr)_t$ values are significantly higher (0·7053–0·7056 vs 0·7046). Lead and Sr isotope ratios are similar to those reported for Site 1137 (Ingle *et al.*, 2002*b*), but the Site 1141 and 1142 basalts exhibit higher (slightly positive) ε_{Nd} values (Figs 3 and 4). Compared with the Site 1138 lavas and the upper two units of Site 1136, the Site 1141 and 1142 rocks have similar $(^{206}Pb/^{204}Pb)_t$ but higher $(^{207}Pb/^{204}Pb)_t$ and $(^{208}Pb/^{204}Pb)_t$.

DISCUSSION

Elemental data for basalt lavas erupted over a 24 Myr time span (Site 1136 at 118–119 Ma, Site 1138 at 100–101 Ma, and Sites 1141 and 1142 at ~95 Ma; Duncan, 2002) show geochemical heterogeneity typical of the Kerguelen Plateau–Broken Ridge LIP (see Davies *et al.*, 1989; Weis *et al.*, 1989; Salters *et al.*, 1992; Mahoney *et al.*, 1995). This heterogeneity is generally interpreted in terms of magma generated from a heterogeneous

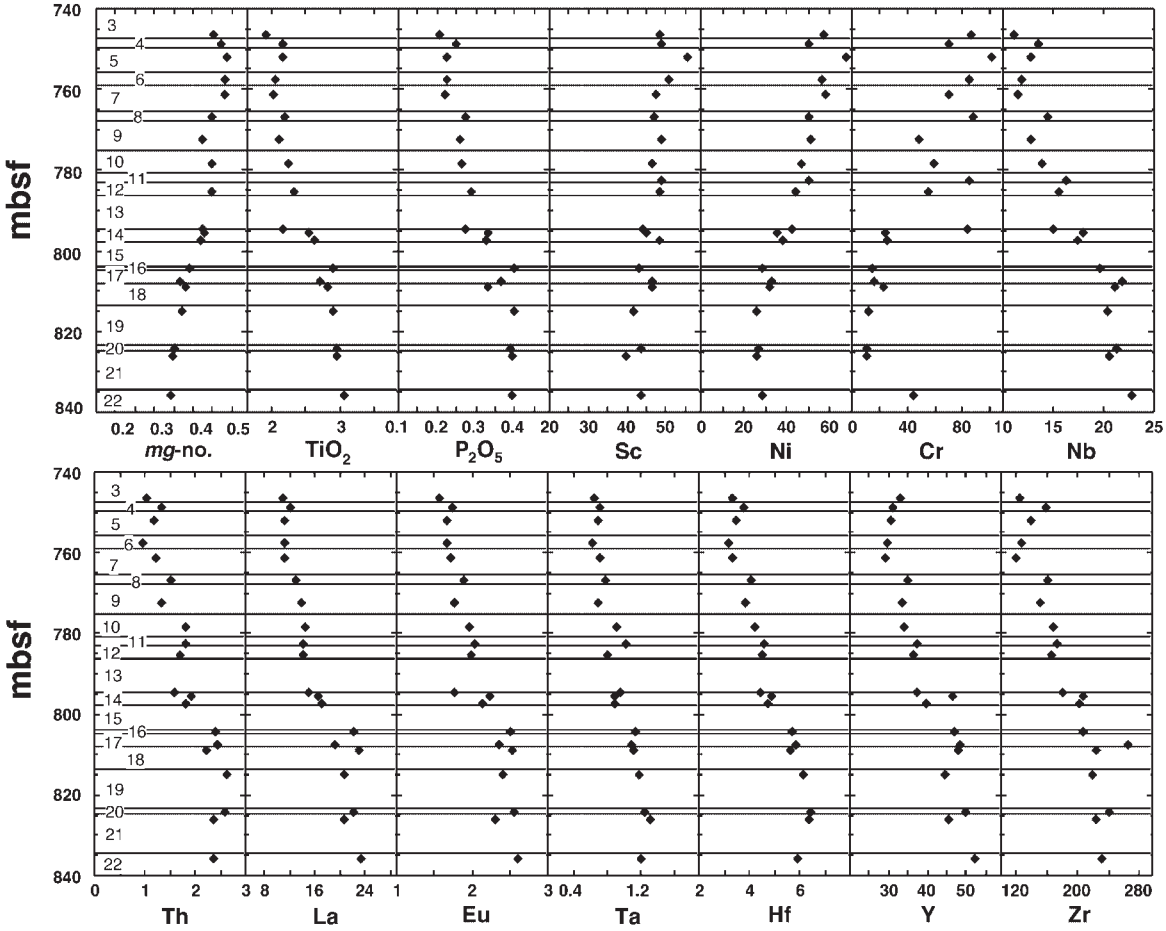

Fig. 6. Downhole chemical variations in the basalt units (Units 3–22) of Site 1138. The unit numbers are given to the left of each panel; mbsf, meters below the sea floor. Oxide abundances are in wt % and element abundances are in ppm.

plume source and which occasionally assimilated small amounts of crustal material. However, the isotope data reported here exhibit surprisingly little overall variation in $(^{206}Pb/^{204}Pb)_t$ and $\varepsilon_{Nd}(t)$ and only modest variation in $(^{87}Sr/^{86}Sr)_t$.

Southern Kerguelen Plateau (SKP)

Four ODP sites drilled into the SKP (Fig. 1) recovered basaltic basement. The basalt units recovered exhibit a wide range of incompatible element and isotopic compositions (Figs 3, 4, and 5a and b; Salters *et al.*, 1992; Storey *et al.*, 1992; Frey *et al.*, 2002). Basement from Site 738 is characterized by a pronounced continental crustal or lithospheric mantle signature (e.g. Storey *et al.*, 1992; Mahoney *et al.*, 1995; Fig. 5b), very different from anything seen at Sites 749 and 750 (see, e.g. Salters *et al.*, 1992; Frey *et al.*, 2002). Frey *et al.* (2002) have invoked a plagioclase-rich lower-crustal end-member to explain the compositions of the Site 750 lavas, including their relatively non-radiogenic Pb isotopes and $[Sr/Nd]_{PM} > 1$. Primitive mantle normalized patterns show that unlike the basalts from Sites 749 and 750, those from Site 1136 (and Site 738) lack peaks at Sr. The three Site 1136 units exhibit Nb depletions, but smaller than those of Site 738 lavas. Unit 3 at Site 1136 exhibits a smooth decrease from Ce to Nb, is enriched in the REE and Y relative to the other two units, and also is distinct isotopically (Figs 3 and 4). Tantalum is enriched relative to Nb in Units 2 and 3 (i.e. Nb/Ta = 12·1–12·6, versus a chondritic value of 17·4 in Unit 1), qualitatively similar to six of the 11 Site 749 and Site 750 lavas studied by Frey *et al.* (2002), which have Nb/Ta = 12·1–14·8 and overlap with values estimated for average continental crust (e.g. Rudnick & Fountain, 1995; Barth *et al.*, 2000; Fig. 5c).

Although seismologic data suggest that some continental crust is present in the northern part of the SKP (Operto & Charvis, 1996), the geochemical data now available indicate that both the influence and types of continental material affecting magmas in the SKP are

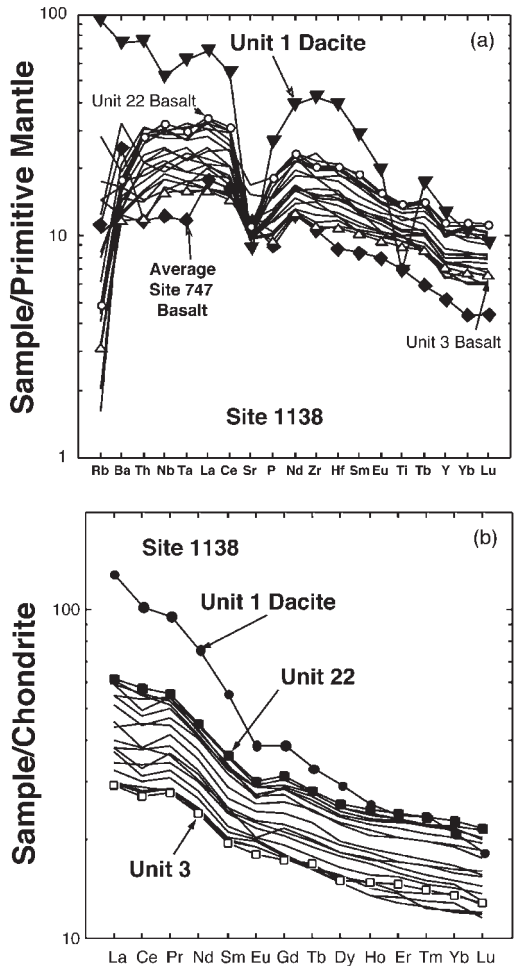

Fig. 7. (a) Primitive mantle normalized incompatible element profiles of the dacite (Unit 1) and basalts (Units 3–22) from Site 1138. Also plotted is the average basalt composition from Site 747 (Salters *et al.*, 1992; Frey *et al.*, 2002). (b) Chondrite-normalized rare earth element profiles of the dacite (Unit 1) and basalts (Units 3–22) from Site 1138. Primitive mantle and chondrite values are from Sun & McDonough (1989).

highly variable. The influence of continental crust and perhaps lithospheric mantle is emphasized when $(La/Nb)_{PM}$ and $(La/Ta)_{PM}$ ratios are plotted against $\Delta 7/4$ and $\Delta 8/4$ (Fig. 9). Although highly positive $\Delta 7/4$ and $\Delta 8/4$ values do not by themselves indicate the involvement of continental material, they are strongly suggestive of such an influence if accompanied by $(La/Nb)_{PM}$ and $(La/Ta)_{PM}$ values significantly greater than one (e.g. Mahoney *et al.*, 1995; Frey *et al.*, 1996).

This is highlighted by the comparison of basalts from each of the SKP drill sites. Site 738 basalts have the highest $\Delta 7/4$ and $\Delta 8/4$ values and the highest $(La/Nb)_{PM}$ and $(La/Ta)_{PM}$ values of ~ 2. Site 749 basalts have the lowest $\Delta 7/4$ and $\Delta 8/4$ values (although they are still positive) and $(La/Nb)_{PM} \sim 1{\cdot}1$, with $(La/Ta)_{PM} \sim 1$. Basalts from Sites 750 and 1136 have similar $\Delta 7/4$ and $\Delta 8/4$ values, but the former have $(La/Nb)_{PM}$ and $(La/Ta)_{PM}$ values $\leqslant 1$. Site 1136 basalts all have $(La/Nb)_{PM}$ between 1·3 and 1·6 and $(La/Ta)_{PM}$ between 1·0 and 1·3 (Fig. 9). The Site 1136 $(La/Nb)_{PM}$ and $\Delta 7/4$ values are similar to those of the Casuarina group of Bunbury Basalt lavas, which have been interpreted as being slightly influenced by continental material (Frey *et al.*, 1996). Units 1 and 2 lavas have elevated $(^{207}Pb/^{204}Pb)_t$ relative to values for the Site 1138 basalts (see below); their relatively high $(La/Nb)_{PM}$ and the marked Pb peaks in their incompatible element patterns (Fig. 5a) are also consistent with minor involvement of continental material of some sort. We conclude that the compositions of Site 1136 basalts likewise have been influenced slightly by continental material.

The highly altered nature and poor recovery of Unit 3 hinder the interpretation of its composition. The elevated REE and Y in this sample are not a result of secondary apatite or calcite because this sample has the same P_2O_5 and Sr contents as other Site 1136 basalts (Table 1; Fig. 5a). Unit 3 has the most positive $\varepsilon_{Nd}(t)$ value (+5·1) of any sample analyzed in this study (Table 2). The high ε_{Nd} is unlikely to be caused by alteration; seawater has negative ε_{Nd} values, and Nd isotopes are resistant to even relatively high levels of alteration. Similarly, the normalized incompatible element profile is difficult to reconcile with alteration. We suggest that Unit 3 at Site 1136 represents a unique component in the source region for this area of the Kerguelen LIP.

Central Kerguelen Plateau (CKP)

Tholeiitic to transitional basalts have been recovered from two drill sites on the CKP at Site 747 and Site 1138, both to the SE of Heard Island (Fig. 1; Storey *et al.*, 1992; Frey *et al.*, 2002). Unlike the Site 747 lavas, those from Site 1138 do not have significant relative depletions in Nb, Ta or Th, and the Site 747 basalts have much lower $\varepsilon_{Nd}(t)$ and $(^{206}Pb/^{204}Pb)_t$ and higher $(^{87}Sr/^{86}Sr)_t$ (Figs 3 and 4). Frey *et al.* (2002) argued that the Site 747 magmas assimilated appreciable amounts of old, lower continental crust, to account for the unusual isotopic characteristics (Figs 3 and 4), the relatively low abundances of Th, Nb, and Ta, and the combination of positive $\Delta 7/4$ and $\Delta 8/4$ values in conjunction with $(La/Nb)_{PM}$ and $(La/Ta)_{PM} > 1$ in these basalts (Figs 7a and 9). In view of the isotopic characteristics and the lack of Nb, Ta, or Th depletions in Site 1138 lavas (Figs 3, 4, 7a, and 9), we infer that there is no significant influence of continental crust in these basalts.

The Site 1138 basalts appear to have experienced substantial plagioclase (Sr and Eu depletions), clinopyroxene (Y depletion), and olivine (25–67 ppm Ni;

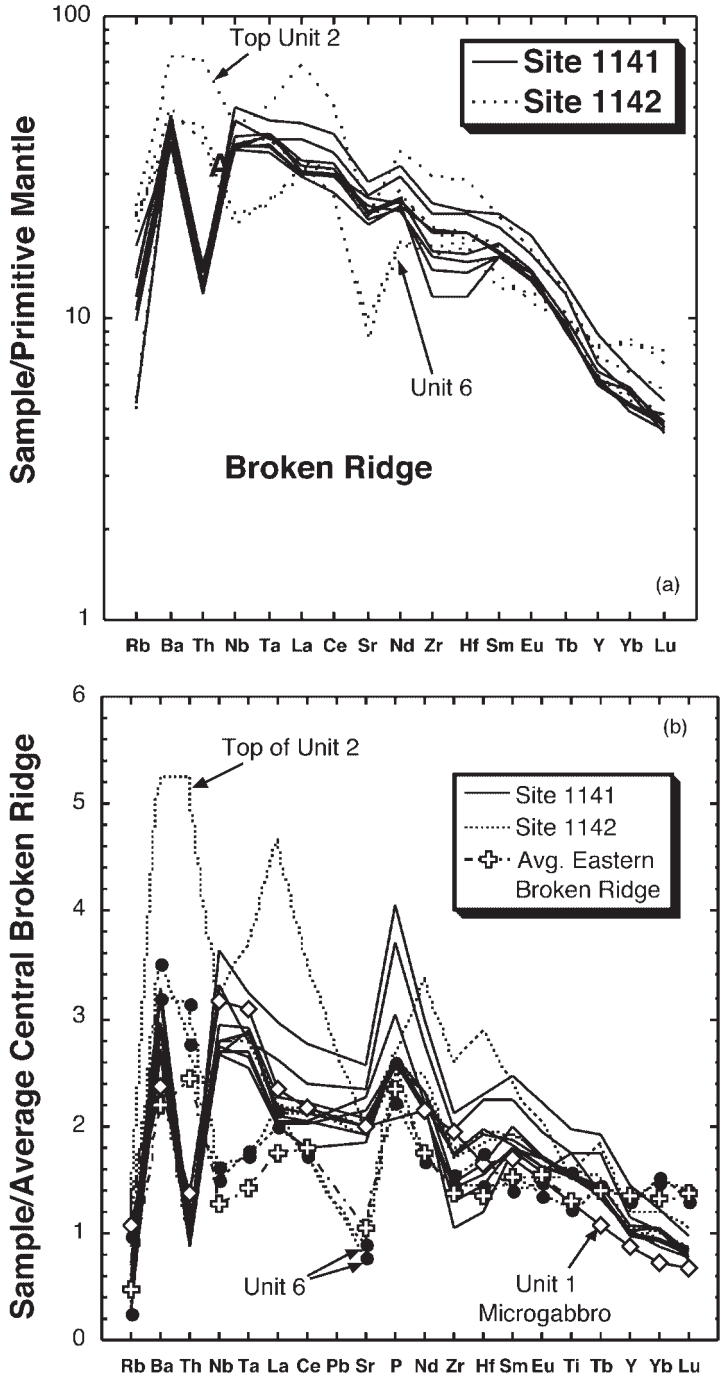

Fig. 8. (a) Primitive mantle normalized incompatible trace element profiles of basalts from Broken Ridge Sites 1141 and 1142. Primitive mantle values are from Sun & McDonough (1989). (b) Comparison of the Broken Ridge lavas with dredge samples reported by Mahoney *et al.* (1995). All data are normalized to the average composition for central Broken Ridge dredge samples. It should be noted that the Leg 183 samples are enriched relative to the dredge samples and that the average composition for eastern Broken Ridge dredge samples is similar to the Site 1142 tholeiite (Unit 6).

Table 1) fractionation, consistent with petrographic observations. The resultant geochemical variations at first sight suggest an evolving magma in a closed system. This is indicated by the combination of: (1) the very small amount of Sr, Nd, and Pb isotopic variation (Figs 3 and 4 and Table 2); (2) the sub-parallel incompatible element

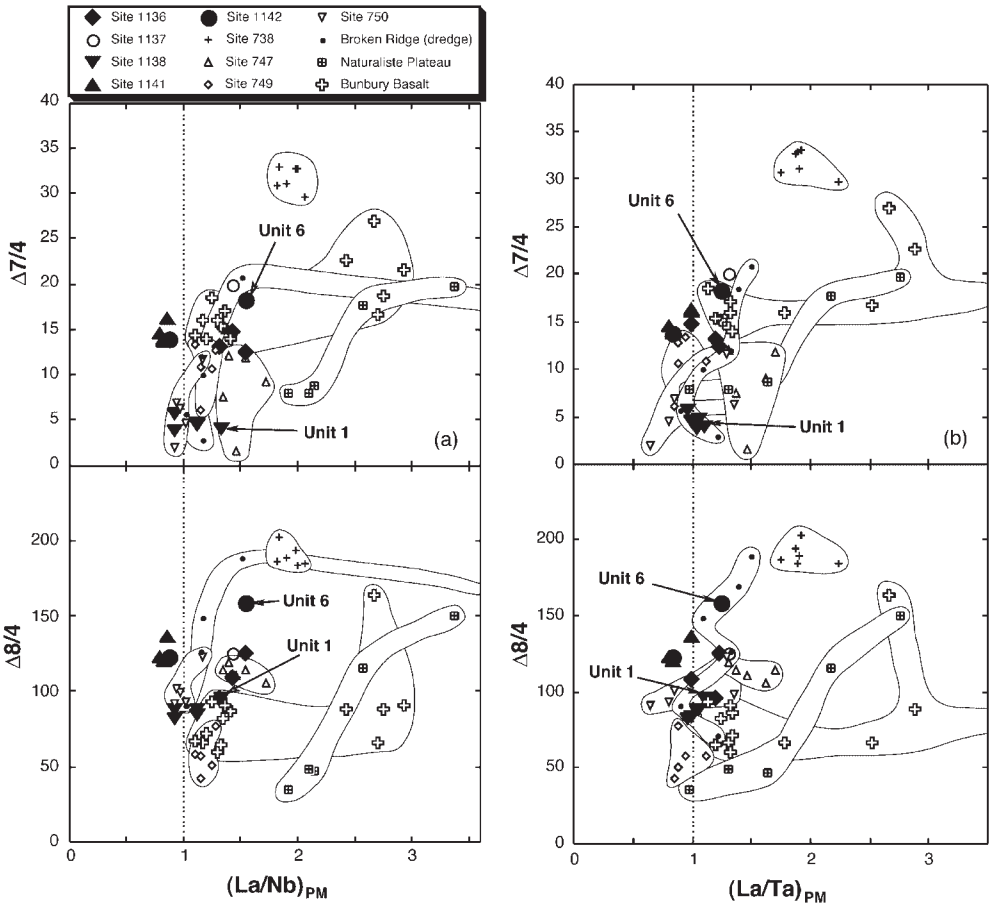

Fig. 9. (a) $(La/Nb)_{PM}$ vs Δ8/4 and Δ7/4; (b) $(La/Ta)_{PM}$ vs Δ8/4 and Δ7/4. A combination of significantly positive Δ8/4 and Δ7/4 values and normalized element ratios >1 is likely to reflect contamination with continental crust. The Site 1138 Unit 1 dacite and Site 1142 Unit 6 tholeiitic basalt are highlighted as, unlike other samples from these sites, they appear likely to record effects of continental crustal contamination. It should be noted that incompatible element ratios for Broken Ridge dredge samples in (a) and for the Bunbury Basalt in (b) extend to values greater than depicted in these diagrams. Data sources: Site 1137, Ingle *et al.* (2002*b*); Site 738, Broken Ridge, and Naturaliste Plateau, Storey *et al.* (1992) and Mahoney *et al.* (1995); Sites 747, 749, and 750, Frey *et al.* (2002); Bunbury Basalt, Frey *et al.* (1996). Primitive mantle values are from Sun & McDonough (1989).

profiles (Fig. 7); (3) a general increase in incompatible element and decrease in compatible element abundances going through the sequence from Unit 3 to Unit 22 (Fig. 6); (4) the lack of any obvious continental lithospheric signature (Figs 7a and 9). However, the range in incompatible element abundances cannot be generated by fractional crystallization of a single magma and, as noted above, the sequence is the stratigraphic opposite of what would be expected. The basalt sequence can be successfully modeled by periodic replenishment of a fractionating basaltic magma (e.g. RFC: O'Hara & Matthews, 1981). The low MgO values of the basalts suggest that the incoming magma was probably not primary, also suggesting that there were multiple magma chambers beneath Site 1138. As noted above, petrography indicates that plagioclase and clinopyroxene are the main phenocryst phases (see Fig. 10) in the sparsely phyric basalts; olivine is a minor phase. Detailed petrography of the opaque phases indicates that titanomagnetite was also a minor yet persistent fractionating phase. Toplis & Carroll (1995) demonstrated that the crystallization of titanomagnetite was dependent on ferric iron abundance requiring an oxygen fugacity at FMQ or higher. The experiments of Toplis & Carroll (1995, 1996) are particularly relevant here as starting compositions are similar to the Site 1138 basalts [i.e. compare SC-1 of Toplis & Carroll (1995) with Unit 7 of Site 1138]. The negative correlation between total Fe and SiO_2 (Fig. 11a) has a similar, although slightly steeper, gradient to that proposed by Toplis & Carroll (1995) for the onset of magnetite saturation in basaltic magmas. However, this would require that the highest SiO_2 magmas would be the most evolved, yet they have the highest *mg*-number. Conversely, there is a positive correlation between total

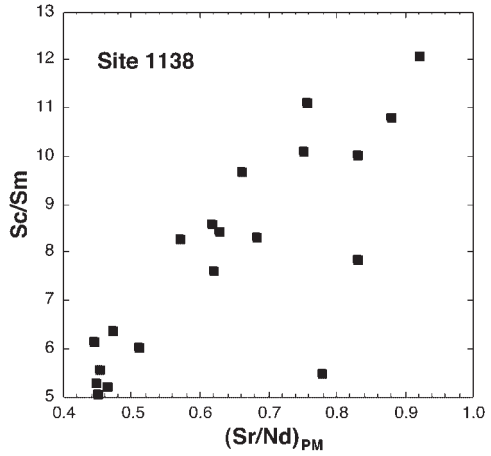

Fig. 10. Plot of Sc/Sm vs $(Sr/Nd)_{PM}$ for the 20 Site 1138 basalt units. The positive correlation is consistent with a crystal fractionation sequence dominated by plagioclase and clinopyroxene.

Fe and TiO_2 (Fig. 11b), and TiO_2 increases with decreasing *mg*-number (Fig. 6). Therefore, the proportion of titanomagnetite on the liquidus was not large enough (i.e. <10%) to promote a decrease in TiO_2 or total Fe contents of the magma. Rather, the crystallization of this phase tempered the increase of Fe (see Toplis & Carroll, 1996, fig. 2a) and TiO_2. Finally, as phenocrysts exhibit resorption features, it suggests titanomagnetite fractionation was inefficient.

Although the downhole correlations are coherent in the basalt lava sequence at Site 1138, element–element correlations are diffuse, suggesting processes other than fractional crystallization are occurring. It may be that this negative correlation between total Fe and SiO_2 represents olivine resorption coupled with the onset of titanomagnetite crystallization (see Toplis & Carroll, 1995; see fig. 12a of Toplis & Carroll, 1996), which produces a steeper gradient on iron–silica correlation plots such as that observed with our data. Such a process would explain the fact that the highest SiO_2 magmas have the highest *mg*-number. Indeed, olivine phenocrysts exhibit resorption features, which we interpret as a result of magmatic evolution that resulted in olivine instability such that it reacted with the magma. At high oxygen fugacities, magnetite is a crystalline product (see Toplis & Carroll, 1995). However, petrography also demonstrates resorption features on clinopyroxene and titanomagnetite phenocrysts, especially in Units 3–10. These we interpret as indicating an influx of new magma into the chamber.

In our RFC model (Fig. 12), we have used petrography as a guide in establishing a fractionating assemblage of plagioclase, clinopyroxene, and titanomagnetite crystallizing in the proportions 32:60:8, which is consistent with the behavior of Eu, Sc, Ni, and TiO_2 abundances as well as with Sc/Sm and $(Sr/Nd)_{PM}$ ratios in the lava sequence (Figs 6 and 10; Table 3). The mass crystallized during each RFC stage is 15%, the mass of magma erupted is 8%, and the mass of magma added is 10%; this combination of parameters represents a shrinking or 'dying' magma chamber, consistent with the drilled sequence being the final set of eruptions in this area of the CKP. The model parameters, including the parental magma composition, have been chosen to best fit the data. We envisage that equilibrium would be disturbed by an influx of parental magma into the chamber, changing the magma composition and causing clinopyroxene and titanomagnetite to be resorbed. The scarcity of olivine would be a result of it being carried up from a lower magma chamber and then resorbed through reaction with the more evolved magma and promoting titanomagnetite crystallization (see Toplis & Carroll, 1995). Therefore, it is not included as a fractionating phase in our model but is treated as a resorbed phase; the phases being resorbed are olivine, clinopyroxene and titanomagnetite in the proportions 1:3:6 (Table 3) and for simplicity we model resorption as a single-stage process. The resorption process accounts for the modest change in Sc (Fig. 6), even though clinopyroxene forms 60% of the fractionating sequence. What is immediately noticeable is that when the Site 1138 basalt data are represented on element–element plots, they do not define a smooth trend from Unit 3 to Unit 22 (Fig. 12). This disjointed sequence of elemental variations is reproduced in our model by varying the amount of phenocryst resorption. Although these results are clearly model dependent, they illustrate that RFC processes can generate the basalt sequence at Site 1138.

The model does not, however, necessarily account for the fact that the entire Site 1138 basalt sequence is the stratigraphic opposite of what would be expected in that the least differentiated units were erupted last (i.e. are at the top; Fig. 6). The criteria used for defining unit boundaries and the orientation of vesicle trains indicate that the sequence is not overturned (Coffin *et al.*, 2000; Keszthelyi, in preparation). A possible explanation could be that the lowermost unit recovered at Site 1138 represents a more highly evolved basalt formed after an extended period of fractional crystallization without replenishment. Later flows would then represent successive influxes of comparatively primitive parental magma, the amount of which would exceed the amount crystallized during the preceding stage (i.e. the reverse of the sequence modeled above). Consecutively more primitive-looking basaltic magmas would be erupted even while phenocrysts continued to be resorbed. This can be modeled by using the most evolved basalt from Site 1138 as the initial magma composition, with the assumed parent from the model defined in Fig. 12 as the incoming magma. Resorption of phenocryst phases and a decrease in the

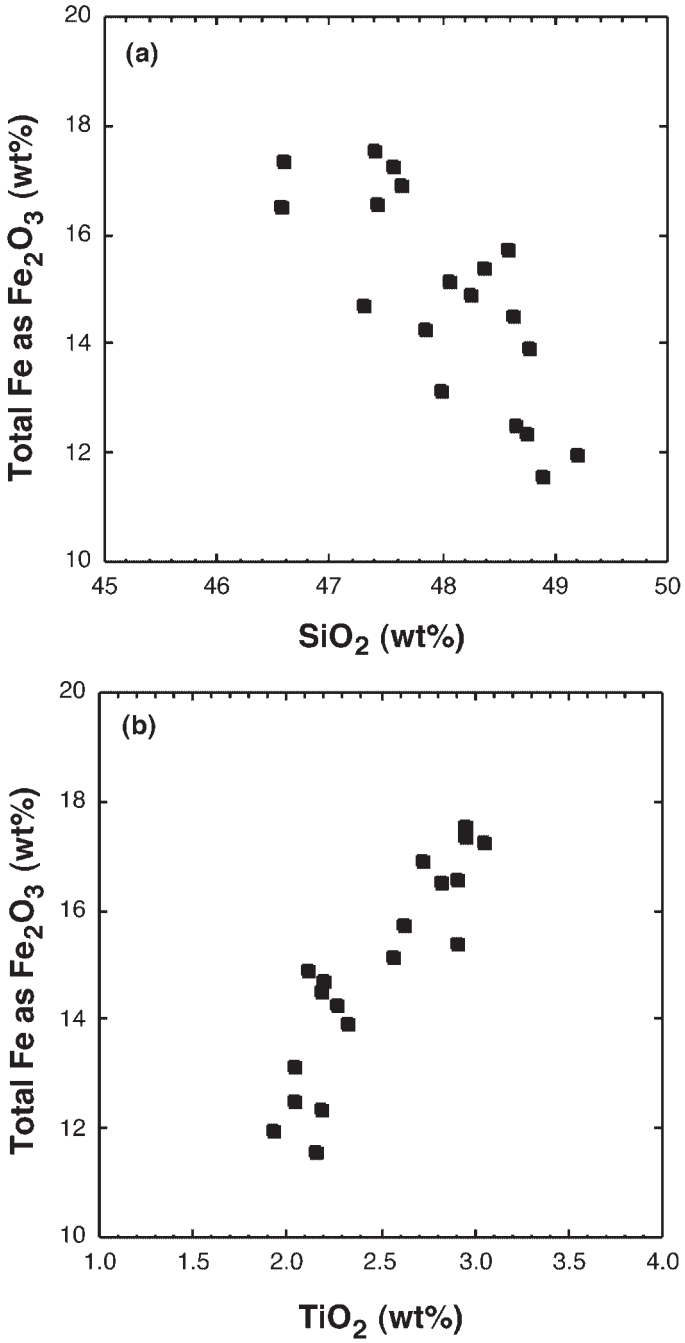

Fig. 11. Plots of total iron (as Fe_2O_3 wt %) vs SiO_2 (a), and TiO_2 (b). The correlations are consistent with titanomagnetite being a liquidus phase during the crystal fractionation of this basalt sequence (see Toplis & Carroll, 1995). (See text for discussion.)

amount of fractional crystallization are required to generate the observed basalt compositions using this approach. Whatever the details of the process(es), it is clear that the system was isotopically essentially homogeneous and that multiple stages of differentiation were required.

The Unit 1 dacite is isotopically distinct from the basalts (Figs 3 and 4). The horizontal displacement of the dacite from the basalts on an $\varepsilon_{Nd}(t)$ vs $(^{87}Sr/^{86}Sr)_t$ diagram (Fig. 3) is unlikely to be caused solely by seawater alteration that was not removed by acid leaching, because the dacite has a high Sr concentration (179·5 ppm in the leached split; 187 ppm in the whole rock) relative to that of seawater ($\sim$8 ppm) and the Sr isotope ratio of $\sim$100 Myr old seawater was only

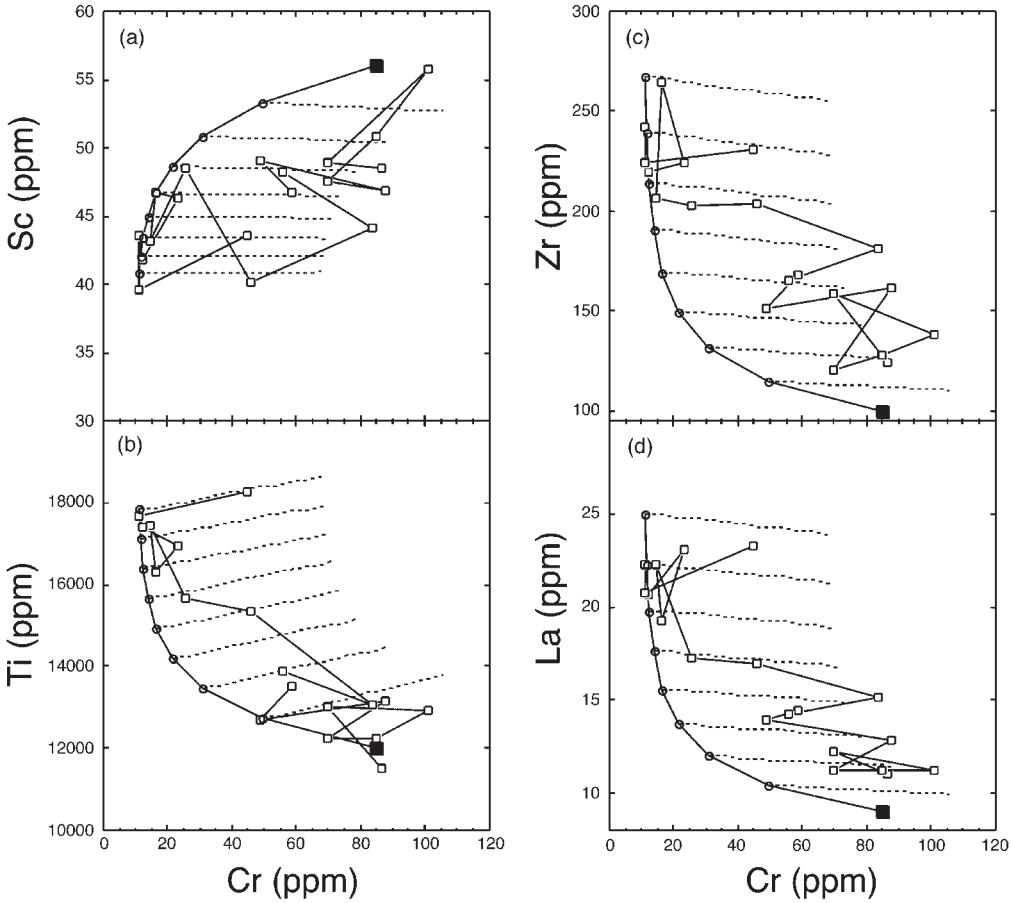

Fig. 12. Modeling of the Site 1138 basalt sequence by replenishment and fractional crystallization (O'Hara & Matthews, 1981). ■, parental magma composition, which is the composition that periodically replenishes the system (Cr 85 ppm; Sc 56 ppm; Ti 12 000 ppm; Zr 100 ppm; La 9 ppm). The continuous line linking the open squares indicates how the actual compositions of successive basaltic units from Site 1138 change. The open circles linked by a continuous line represent individual replenishments after periods of fractional crystallization during which there is no resorption of crystallized phases. The fractionating assemblage is plagioclase, clinopyroxene, and titanomagnetite crystallizing in the proportions 32:60:8. The mass crystallized during each RFC stage is 15%, the mass of magma erupted is 8% and the mass of magma added is 10%. The dashed lines emanating from each open circle indicate how the magma composition is changed as crystalline phases (olivine, clinopyroxene, and titanomagnetite; see text for discussion) are resorbed in the proportions 1:3:6. The furthest end of each of these dashed lines from the open circle represents 5% resorption. Using this model, the Site 1138 basalt sequence can be approximated by eight replenishment cycles followed by variable (0–5%) resorption of the crystallized phases. Partition coefficients were taken from the compilations of Rollinson (1993) and Green (1994).

~0·7073 (e.g. Burke *et al.*, 1982), close to the 0·7065 value of the dacite itself. The trace element data (Table 1; Fig. 7) show that the dacite is more LREE enriched than the basalts, exhibits a larger Sr depletion, and exhibits depletions in Nb and Ta relative to La. We speculate that the dacite could be the product of crystal fractionation of a basaltic magma like those represented by Units 3–22, as oxide fractionation can potentially generate magmas with $(La/Nb)_{PM}$ and $(La/Ta)_{PM}$ ratios slightly above unity (Rollinson, 1993; Green, 1994). However, the magnitude of the LREE enrichment in the dacite is slightly greater than can be achieved from fractional crystallization alone. Its high $(^{87}Sr/^{86}Sr)_t$ and lower Pb isotope ratios suggest open-system crystal fractionation and possibly reflect the influence of some continental lithospheric material.

Broken Ridge

The presence of alkalic lavas overlying a tholeiitic basalt at Site 1142, coupled with the fact that all of the igneous rocks dredged from Broken Ridge are tholeiitic basalts, suggests that a main tholeiitic phase of volcanism may have been capped by a late-stage alkalic carapace in the Broken Ridge portion of the original CKP. The sequence of volcanism at Broken Ridge would thus be similar to that observed in some ocean islands. For example,

Table 3: Parameters for the RFC modeling of the Site 1138 basalts (Units 3–22)

Element	Parental composition	Resorbed component*	Partition coefficients			
			Cpx	Plag	T-Mag	Olivine
Cr	85	1173	5	0·033	20	3
Sc	56	41·8	2·2	0·007	0·1	0·27
Ti	12000	33864	0·4	0·04	4·5	0·01
Zr	100	6·6	0·1	0·048	0·06	0·001
La	9	0·9	0·034	0·042	0·15	0·0001
Mass crystallized:	15%					
Mass erupted:	8%					
Mass replenished:	10%					
Mineral phases	Crystallized assemblage (%)	Resorbed assemblage (%)				
Plagioclase	32	—				
Clinopyroxene	60	30				
Titanomagnetite	8	60				
Olivine	—	10				

*The quoted composition of the resorbed component is averaged over the RFC process and calculated from equilibrium liquids. Cpx, clinopyroxene; Plag, plagioclase; T-Mag, titanomagnetite. Partition coefficients taken from Rollinson (1993) and Green (1994); titanomagnetite partition coefficients are taken as being equivalent to those for magnetite.

late-stage alkalic lavas commonly cap main-stage tholeiitic (shield-building) basalts on Hawaiian volcanoes (e.g. Clague & Dalrymple, 1987). At Broken Ridge, the small amount of variation in, for example, Zr/Y, Sc/Sm, and La/Yb (i.e. Fig. 13), is interpreted to represent a change in degree of partial melting of a spinel peridotite source, rather than a change to a deeper, garnet-bearing source with a concomitant decrease in degree of partial melting. One sample with distinctly high $(La/Yb)_{PM}$ and Zr/Y (Fig. 13) is from the Site 1142 talus deposit (Unit 2).

The alkalic basalts recovered from Broken Ridge during Leg 183 are distinct from the dredged tholeiites in that they contain higher abundances of Nb and Ta and also a marked Th depletion (Fig. 8). However, tholeiitic Unit 6 and a pebble from the top sample of Unit 2 from Site 1142 are similar to the dredge samples in that they have $(La/Nb)_{PM} > 1$ and $(Nb/Th)_{PM} < 1$ (Fig. 8). The dredge samples exhibit a broader range of Sr, Nd, and Pb isotopic compositions [e.g. $\varepsilon_{Nd}(t) = -2{\cdot}7$ to $+3{\cdot}4$] that encompasses the small range defined by the Site 1141 and 1142 samples [which all have, for example, $\varepsilon_{Nd}(t) = +0{\cdot}3$ to $+0{\cdot}7$; Fig. 3].

Mahoney *et al.* (1995) interpreted the low-$\varepsilon_{Nd}(t)$ dredge samples, particularly from Dredge 8 on the eastern Broken Ridge, to contain continent-derived material on the basis of combined Th/Ta, La/Nb, La/Ta, and Δ7/4 and Δ8/4. The similarity in incompatible element profiles of the Unit 6 tholeiite from Site 1142 to the eastern Broken Ridge dredge samples (Fig. 8b) suggests it may also contain a small amount of continent-derived material. The two samples analyzed from this unit have $(La/Ta)_{PM}$ and $(La/Nb)_{PM} > 1$, similar to the dredge samples, the Bunbury Basalt, and some Naturaliste Plateau lavas (Fig. 9). The Broken Ridge lavas recovered during Leg 183 have similar $(^{206}Pb/^{204}Pb)_t$ to those from Site 1137 (Figs 3 and 4), which are considered to contain a component of continental crust (Ingle *et al.*, 2002*a*, 2002*b*). However, except for the tholeiitic Unit 6 of Site 1142, the lavas from Sites 1141 and 1142 have lower $(^{207}Pb/^{204}Pb)_t$ and $(^{208}Pb/^{204}Pb)_t$ (Fig. 4 and Table 2). The lack of a continental influence in the alkalic basalts is emphasized by trace element ratios (Fig. 9). The alkalic samples from Sites 1141 and 1142 have $(La/Ta)_{PM}$ and $(La/Nb)_{PM} \sim 1$, but like Kerguelen Archipelago lavas, still have elevated Δ7/4 and Δ8/4. Such features are

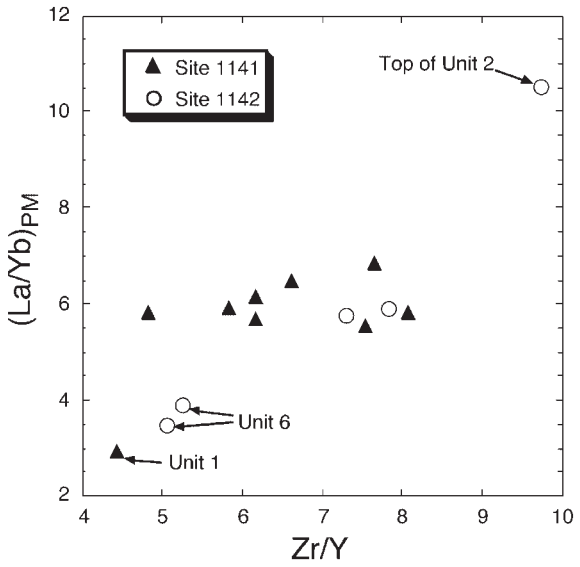

Fig. 13. Zr/Y vs $(La/Yb)_{PM}$ for the Leg 183 Broken Ridge samples showing relatively limited variation in these ratios, which can be attributed to changes in degree of partial melting rather than a change from spinel to garnet peridotite as the source. The sample labeled 'Top of Unit 2' is a pebble from an inferred talus deposit (breccia) at Site 1142 and has probably been derived. The sample labeled 'Unit 1' is the micrograbbro from Site 1141, and those labeled 'Unit 6' are from the tholeiitic unit at Site 1142. Primitive mantle values are from Sun & McDonough (1989).

likely to be intrinsic to the Kerguelen plume (see Weis *et al.*, 1989, 1991; Frey & Weis, 1995, 1996).

End-members in Kerguelen Plateau development

Most recent workers have argued that the Kerguelen Plateau was constructed during the early stages of activity of a long-lived mantle plume (e.g. Davies *et al.*, 1989; Weis *et al.*, 1989, 1991; Coffin, 1992; Storey *et al.*, 1992; Frey & Weis, 1995; Mahoney *et al.*, 1995). As noted above, the geochemistry of the magmatic products of the Cretaceous–Recent Kerguelen hotspot system generally has been described in terms of variable mixtures of a dominant plume component (with ε_{Nd} near zero), a secondary plume component (isotopically similar to Amsterdam–St. Paul), possibly a small amount of Indian MORB-type mantle, and the incorporation of variable amounts of heterogeneous continental lithospheric material. The isotope data reported here are from rocks that span ~24 Myr yet exhibit little variation in $(^{206}Pb/^{204}Pb)_t$ and $\varepsilon_{Nd}(t)$ and, except for the Site 1138 dacite, only modest variation in $(^{87}Sr/^{86}Sr)_t$. A much wider range of Nd and Sr isotopic values is documented for other Kerguelen Plateau and Broken Ridge rocks, as well as Naturaliste Plateau and Rajmahal Traps lavas. Together with our Leg 183 rocks, these same lavas also encompass a wide range of $^{208}Pb/^{204}Pb$ and $^{207}Pb/^{204}Pb$ values. Although not all values are age-corrected, SKP lavas from Sites 738, 749, and 1136, CKP lavas from Sites 1137 and 1138, Broken Ridge lavas from Sites 1141 and 1142, and many of the dredged samples, Rajmahal basalts, and Naturaliste Plateau lavas are characterized by surprisingly limited variation in $^{206}Pb/^{204}Pb$, between about 17·8 and 18·1. This range probably represents the ~120–90 Ma composition of the dominant material of the Kerguelen hotspot mantle source. Moreover, much of the continental-type material that affected many of these magmas, such as those at Sites 738 (Mahoney *et al.*, 1995) and 1137 (Ingle *et al.*, 2002*b*) must have had $^{206}Pb/^{204}Pb$ in broadly this same range.

To further evaluate the different components involved in magmatism related to the Kerguelen hotspot, we use incompatible element ratios in conjunction with isotope data. The element ratios used are relatively insensitive to moderate to large degrees of partial melting and to fractional crystallization processes, and thus should approximately represent source compositions or, in the case of mixed magmas, should represent mixtures of end-member source ratios. In general, Nb/Y vs Zr/Y data for the basalts from Sites 1136, 1138, 1141, and 1142 plot in the Iceland field in Fig. 14a (see Fitton *et al.*, 1997). The CKP basalts have generally higher Zr/Y and Nb/Y than basalts from the SKP basement sites. Probable basaltic products of the Kerguelen hotspot known to reflect a continental lithospheric influence, such as the Bunbury Basalt (Frey *et al.*, 1996), Rajmahal Traps (Kent *et al.*, 1997), Naturaliste Plateau, and Site 738 (Storey *et al.*, 1992; Mahoney *et al.*, 1995) define sub-parallel trends extending below the Iceland array. Data for hawaiites from Afanasy Nikitin Rise (a small plateau 3560 km NNW of Site 1141), which record a large continental lithospheric mantle or lower-crustal influence (Mahoney *et al.*, 1996; Borisova *et al.*, 2001), fall slightly beneath the Iceland array. Data for the alkalic lavas of Broken Ridge Sites 1141 and 1142 plot near those for St. Paul Island (Frey & Weis, 1995).

The presence of continental components in some of the Kerguelen LIP basalts is again evident in Fig. 14b in that many lavas have $(Th/Ta)_{PM}$ and $(La/Nb)_{PM} > 1$. The influence of continental material on the Leg 183 rocks is comparatively subtle. For example, the Site 1136 samples exhibit elevated $(La/Nb)_{PM}$, but $(Th/Ta)_{PM}$ is close to unity, similar to the situation for the Site 747 lavas (Frey *et al.*, 2002). Some estimates of average lower continental crust composition have $(Th/Ta)_{PM}$ and $(Th/Nb)_{PM} \sim 1$, with $(La/Nb)_{PM} > 1$ (e.g. Weaver & Tarney, 1984; Rudnick & Fountain, 1995; Figs 5c, 14b, and 15a). Lower continental crust can be a major contaminant of continental flood basalts (e.g. Peng *et al.*, 1994) and the influence of such material has been proposed at several places in the SKP as well as at Site 747 in the CKP

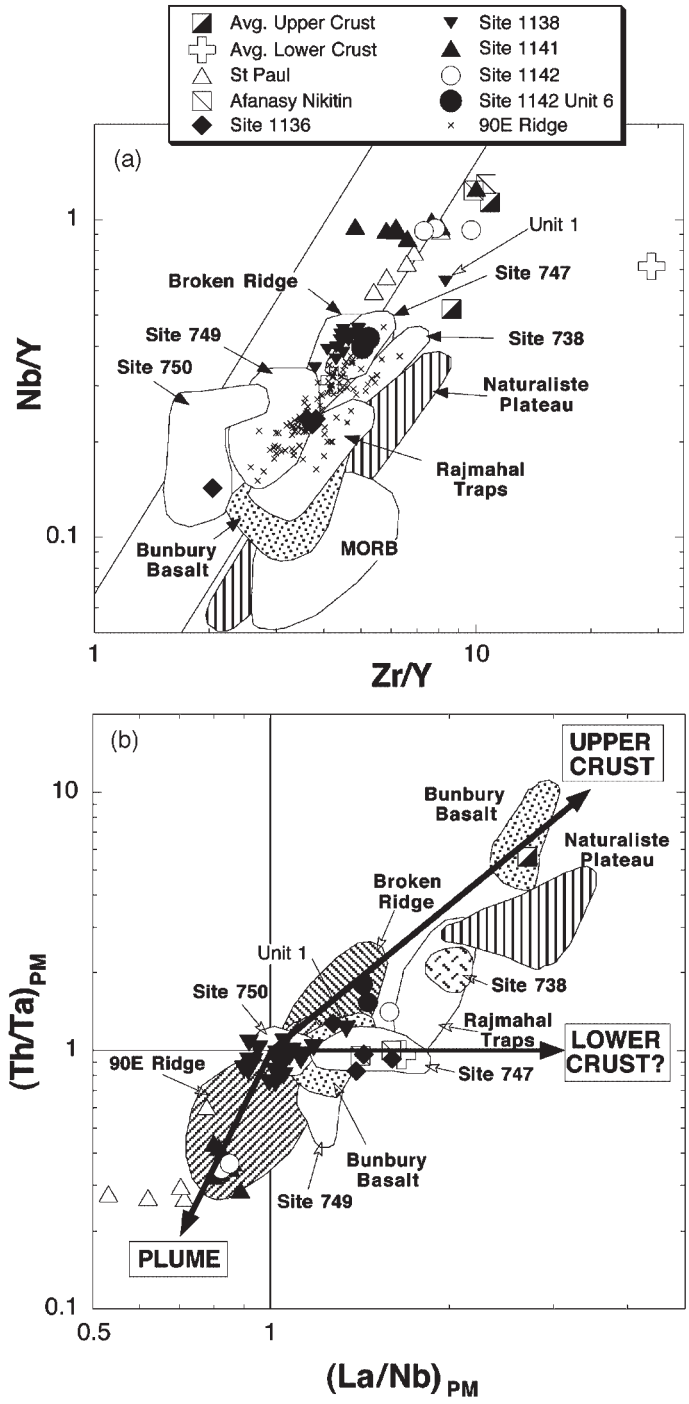

Fig. 14. Incompatible element ratio plots for the magmatic products of the Kerguelen hotspot and other likely Kerguelen hotspot-related rocks (Rajmahal Traps, Bunbury Basalt, Naturaliste Plateau). (a) Nb/Y vs Zr/Y (see Fitton *et al.*, 1997). The Icelandic lava data fall between the parallel lines, but MORB and continental crust lie below the lower line. (b) $(Th/Ta)_{PM}$ vs $(La/Nb)_{PM}$, demonstrating probable effects of continental material on hotspot-derived magmatic products. Data sources are as follows: Broken Ridge, Mahoney *et al.* (1995); Ninetyeast Ridge, Frey *et al.* (1991), Saunders *et al.* (1991), and Frey & Weis (1995); Site 738, Mehl *et al.* (1991), Frey & Weis (1995), and Mahoney *et al.* (1995); Sites 747, 749, and 750, Salters *et al.* (1992), Storey *et al.* (1992), and Frey *et al.* (2002); Naturaliste Plateau, Storey *et al.* (1992) and Mahoney *et al.* (1995); Bunbury Basalt, Storey *et al.* (1992) and Frey *et al.* (1996); Rajmahal Traps, Kent *et al.* (1997); St Paul Island, Frey & Weis (1995); Afanasy Nikitin Rise, Mahoney *et al.* (1996); average continental crust estimates, Weaver & Tarney (1984) and Rudnick & Fountain (1995). Primitive mantle values are from Sun & McDonough (1989). 'Unit 1' denotes the dacite from Site 1138.

(Frey *et al.*, 2002). We suggest that Units 1 and 2 at Site 1136 may have been slightly contaminated by material similar to average lower continental crust. The Site 1138 dacite plots with the Site 1136 basalts (Units 1 and 2) in Figs 14b and 15a, suggesting it also has been slightly contaminated with such material. Data for the Site 1142 tholeiitic samples (Unit 6) and the upper sample from the talus deposit (Unit 2) plot together and are distinct from data for other basalts from Sites 1141 and 1142 (Figs 14b and 15). On the basis of these diagrams, it is likely that these lavas have been slightly contaminated with material similar to average upper crust. The other Leg 183 Broken Ridge lavas have both $(La/Nb)_{PM}$ and $(Th/Ta)_{PM}$ <1; they plot at the end of the Ninetyeast Ridge field, close to that for St. Paul.

According to the now-standard plume head–plume tail model, as the magmas supplied by the plume head are exhausted, there may be a change in chemical and isotopic composition of lavas as the plume tail phase of hotspot development begins (e.g. Campbell & Griffiths, 1990). We postulate that the alkalic lavas at the top of basement at Sites 1141 and 1142 most closely represent the Cretaceous composition of an important end-member in the Kerguelen plume tail. In terms of incompatible trace element ratios, we see no evidence in our Leg 183 data for a plume component with characteristics resembling those of Amsterdam and St. Paul. This is demonstrated in Figs 3, 4, 14b, and 15. In addition, the alkalic lavas from the Leg 183 Broken Ridge sites consistently plot at one end of the array defined by lavas generated by the Kerguelen hotspot (Figs 14b and 15). Weis *et al.* (1993) concluded that if the isotope compositions of the youngest lavas in the SE province of the Kerguelen Archipelago best represented the modern plume signature, then it would be $^{87}Sr/^{86}Sr = 0{\cdot}7054$–$0{\cdot}7058$, $\varepsilon_{Nd} = -0{\cdot}2$ to $-2{\cdot}9$, $^{206}Pb/^{204}Pb = 18{\cdot}06$–$18{\cdot}27$, $^{207}Pb/^{204}Pb = 15{\cdot}54$–$15{\cdot}58$, and $^{208}Pb/^{204}Pb = 38{\cdot}68$–$39{\cdot}16$ (see also Weis *et al.*, 1998). The 95 Ma alkalic basalts from Sites 1141 and 1142 have $(^{87}Sr/^{86}Sr)_t = 0{\cdot}70533$–$0{\cdot}70556$, $\varepsilon_{Nd}(t) = +0{\cdot}3$ to $+0{\cdot}5$, $(^{206}Pb/^{204}Pb)_t = 17{\cdot}989$–$18{\cdot}022$, $(^{207}Pb/^{204}Pb)_t = 15{\cdot}586$–$15{\cdot}611$, and $(^{208}Pb/^{204}Pb)_t = 38{\cdot}593$–$38{\cdot}770$ (Table 2). The difference in $^{206}Pb/^{204}Pb$ values between young and old compositions is consistent with nearly 100 Myr of radiogenic ingrowth in a plume source possessing modest $^{238}U/^{204}Pb$ ratios (5–16); likewise, assuming slight LREE enrichment in the plume source mantle ($^{147}Sm/^{144}Nd \sim 0{\cdot}16$), then a decrease in ε_{Nd} in 100 Myr of $\sim 0{\cdot}5$ or so would be expected. However, the $(^{207}Pb/^{204}Pb)_t$ values of the Broken Ridge alkalic lavas are greater than those in the postulated present-day plume, which thus cannot be explained solely by radioactive decay over time.

The older ($\sim$101 Ma) Site 1138 basalts may represent a major mantle source in the plume head. They possess nearly primitive mantle ε_{Nd} and $^{87}Sr/^{86}Sr$ values and,

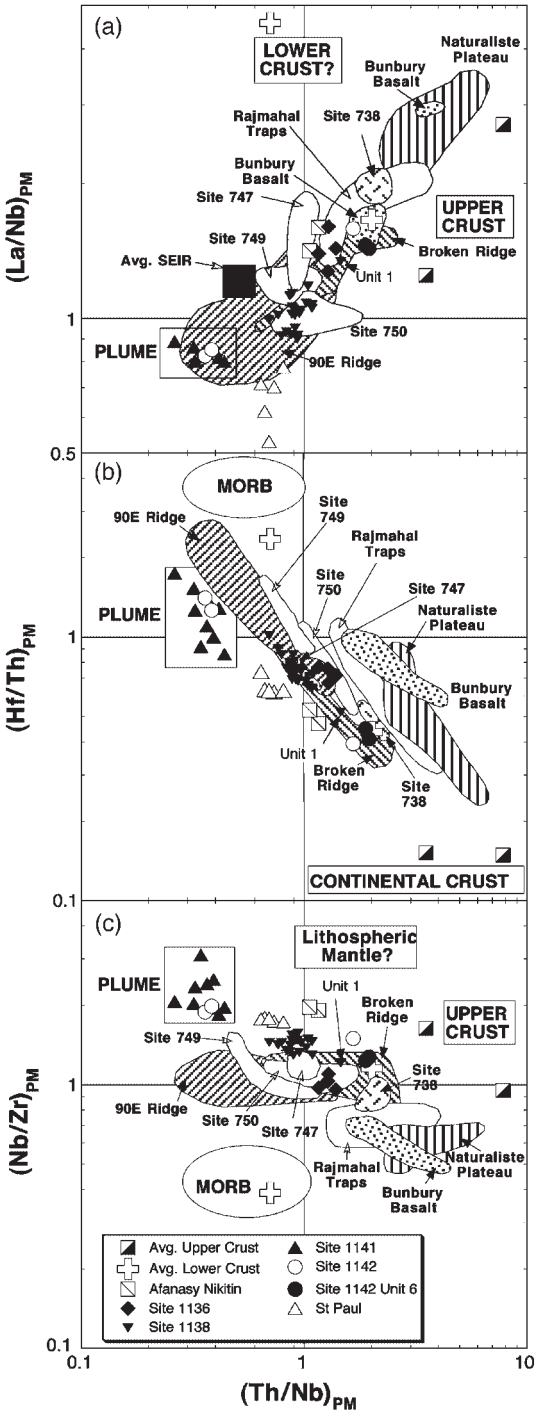

Fig. 15. Primitive mantle normalized element ratio plots with some possible end-member compositions that may have been involved in formation of the Kerguelen large igneous province. Data sources as in Figs 13 and 14. 'Unit 1' denotes the Unit 1 dacite from Site 1138. Southeast Indian Ridge (SEIR) Nb, Th, and La data are from Mahoney *et al.* (2002).

unlike the Site 1141 and 1142 lavas, also have Pb isotopic compositions in the range of primitive mantle estimates (e.g. Galer & Goldstein, 1996). Furthermore, many incompatible element ratios of the Site 1138 basalt units are close to estimated primitive mantle values (Figs 14b and 15).

CONCLUSIONS

Leg 183 lavas formed in association with the early Kerguelen hotspot in the SKP at Site 1136 (118–119 Ma), the CKP at Site 1138 (100–101 Ma), and the Broken Ridge portion of the CKP at Site 1142 (~95 Ma) provide evidence of only small inputs of continental material, unlike rocks from some regions of the Kerguelen Plateau and Broken Ridge (e.g. Site 738 on the SKP and dredge samples from Broken Ridge). The continental influence is inferred from the combination of elevated $\Delta 7/4$ and $\Delta 8/4$ combined with a Nb depletion. The Site 1138 basalts formed through an RFC process with varying degrees of resorption of clinopyroxene, olivine, and titanomagnetite, with little or no influence from continental lithosphere. Their age-corrected isotope ratios and ratios of highly incompatible, alteration-resistant elements are close to primitive mantle estimates (Galer & Goldstein, 1996), and these rocks may be the melt products of a major component in the Kerguelen plume head. Likewise, combined isotopic and trace element data indicate little or no continental lithospheric influence in the alkalic lavas capping Broken Ridge Sites 1141 and 1142. Although these alkalic lavas exhibit elevated $\Delta 7/4$ and $\Delta 8/4$ Pb signatures, they do not contain any associated Nb (or Ta) depletions, hence we interpret the isotopic signature as being of mantle origin and they are likely to represent, in relatively pure form, the composition of a major component of the Cretaceous Kerguelen plume tail. The estimated isotopic composition of late Cenozoic Kerguelen plume mantle is similar, but cannot be related to this Cretaceous composition solely by radioactive decay and ingrowth.

ACKNOWLEDGEMENTS

We are deeply indebted to the officers and crew of the R.V. *JOIDES Resolution* for their help and professionalism in obtaining drill cores during ODP Leg 183. Barry Weaver, Bill White, and Fred Frey provided detailed and thoughtful reviews that greatly improved the quality of this paper and are gratefully acknowledged. The editorial skills of and discussions with Fred Frey and Paul Wallace also greatly enhanced the quality of this contribution. We thank R. Carmody for assistance with the isotopic work and J. Jain for assistance with the ICP-MS analyses. This research used samples and data provided by the Ocean Drilling Program (ODP). The ODP is sponsored by the US National Science Foundation (NSF) and participating countries under the management of Joint Oceanographic Institutions (JOI), Inc. Funding for this research was provided by grants from the United States Science Support Program to C.R.N. and J.J.M.

REFERENCES

Baksi, A. K., Ray Barman, T., Paul, D. K. & Farrar, E. (1987). Widespread early Cretaceous flood basalt volcanism in Eastern India: geochemical data from the Rajmahal–Bengal–Sylhet traps. *Chemical Geology* **63**, 133–141.

Barling, J., Goldstein, S. L. & Nicholls, I. A. (1994). Geochemistry of Heard Island (southern Indian Ocean): characterization of an enriched mantle component and implications for enrichment of the sub-Indian Ocean mantle. *Journal of Petrology* **35**, 1017–1053.

Barron, J. A., Larsen, B., Baldauf, J. G., *et al.* (eds) (1989). *Proceedings of the Ocean Drilling Program, Initial Reports*, 119. College Station, TX: Ocean Drilling Program.

Barth, M. G., McDonough, W. F. & Rudnick, R. L. (2000). Tracking the budget of Nb and Ta in continental crust. *Chemical Geology* **165**, 197–213.

Borisova, A. Yu., Belyatsky, B. V., Portnyagin, M. V. & Sushchevskaya, N. M. (2001). Petrogenesis of olivine-phyric basalts from the Aphanasey Nikitin Rise: evidence for contamination by cratonic lower continental crust. *Journal of Petrology* **42**, 277–319.

Burke, W. H., Denison, R. E., Hetherington, E. A., Koepnick, R.-B., Nelson, H. F. & Otto, J. B. (1982). Variation of seawater $^{87}Sr/^{86}Sr$ throughout Phanerozoic time. *Geology* **10**, 516–519.

Campbell, I. H. & Griffiths, R. W. (1990). Implications of mantle plume structure for the evolution of flood basalts. *Earth and Planetary Science Letters* **99**, 79–93.

Charvis, P., Recq, M., Operto, S. & Brefort, D. (1995). Deep structure of the northern Kerguelen Plateau and hotspot-related activity. *Geophysical Journal International* **122**, 899–924.

Charvis, P., Operto, S., Lesne, O. & Royer, J. (1997). Velocity structure of the Kerguelen volcanic province from wide-angle seismic data: petrological implications. *EOS Transactions, American Geophysical Union* **78**, F711.

Clague, D. A. & Dalrymple, G. B. (1987). The Hawaiian–Emperor volcanic chain, Part I, Geologic evolution. *US Geological Survey Professional Paper* **1350**, 5–54.

Coffin, M. F. (1992). Emplacement and subsidence of Indian Ocean plateaus and submarine ridges. In: Duncan, R. A., Rea, D. K., Kidd, R. B., von Rad, U. & Weissel, J. J. (eds) *Synthesis of Results from Scientific Drilling in the Indian Ocean. Geophysical Monograph, American Geophysical Union* **70**, 115–125.

Coffin, M. F., Munschy, M., Colwell, J. B., Schlich, R., Davies, H. L. & Li, Z.-G. (1990). Seismic stratigraphy of the Raggatt Basin, southern Kerguelen Plateau: tectonic and paleoceanographic implications. *Geological Society of America Bulletin* **102**, 563–579.

Coffin, M. F., Frey, F. A., Wallace, P. J., *et al.* (eds) (2000). *Proceedings of the Ocean Drilling Program, Initial Reports*, 183 (CD ROM). College Station, TX: Ocean Drilling Program.

Coffin, M. F., Pringle, M. S., Duncan, R. A., Gladczenko, T. P., Storey, M., Müller, R. D. & Gahagan, L. A. (2002). Kerguelen hotspot magma output since 130 Ma. *Journal of Petrology* **43**, 1121–1139.

Davies, H. L., Sun, S.-S., Frey, F. A., Gautier, I., McCulloch, M. T., Price, R. C., Bassias, H. L., Klootwijk, C. T. & Leclaire, L. (1989). Basalt basement from the Kerguelen Plateau and the trail of a Dupal plume. *Contributions to Mineralogy and Petrology* **103**, 457–469.

Dosso, L. & Rama Murthy, V. (1980). A Nd isotopic study of the Kerguelen Islands: inferences on enriched oceanic mantle sources. *Earth and Planetary Science Letters* **48**, 268–276.

Dosso, L., Vidal, P., Cantagrel, J. M., Lameyre, J., Marot, A. & Zimine, S. (1979). Kerguelen: continental fragment or oceanic island? Petrology and isotope geochemistry evidence. *Earth and Planetary Science Letters* **43**, 46–60.

Dosso, L., Bougault, H., Beuzart, P., Calvez, J.-Y. & Joron, J.-L. (1988). The geochemical structure of the South-East Indian Ridge. *Earth and Planetary Science Letters* **88**, 47–59.

Duncan, R. A. (2002). A time frame for construction of the Kerguelen Plateau and Broken Ridge. *Journal of Petrology* **43**, 1109–1119.

Fitton, J. G., Saunders, A. D., Norry, M. J., Hardarson, B. S. & Taylor, R. N. (1997). Thermal and chemical structure of the Iceland plume. *Earth and Planetary Science Letters* **153**, 197–208.

Frey, F. A. & Weis, D. (1995). Temporal evolution of the Kerguelen plume: geochemical evidence from ~38 to 82 Ma lavas forming the Ninetyeast Ridge. *Contributions to Mineralogy and Petrology* **121**, 12–28.

Frey, F. A. & Weis, D. (1996). Reply to the Class *et al.* discussion of 'Temporal evolution of the Kerguelen plume: geochemical evidence from ~38 to 82 Ma lavas forming the Ninetyeast Ridge'. *Contributions to Mineralogy and Petrology* **124**, 104–110.

Frey, F. A., Dickey, J. S. J., Thompson, G. & Bryan, W. B. (1977). Eastern Indian Ocean DSDP sites: correlations between petrography, geochemistry and tectonic setting. In: Heirtzler, J. R., *et al.* (eds) *Indian Ocean Geology and Biostratigraphy*. Washington, DC: American Geophysical Union, pp. 189–257.

Frey, F. A., Jones, W. B., Davies, H. & Weis, D. (1991). Geochemical and petrologic data for basalts from Sites 756, 757, and 758: implications for the origin and evolution of Ninetyeast Ridge. In: Weissel, J., Peirce, J., Taylor, E. & Alt, J. (eds) *Proceedings of the Ocean Drilling Program, Scientific Results*, 121. College Station, TX: Ocean Drilling Program, pp. 611–659.

Frey, F. A., McNaughton, N. J., Nelson, D. R., deLaeter, J. R. & Duncan, R. A. (1996). Petrogenesis of the Bunbury Basalt, Western Australia: interaction between the Kerguelen plume and Gondwana lithosphere? *Earth and Planetary Science Letters* **144**, 163–183.

Frey, F. A., Coffin, M. F., Wallace, P. J., Antretter, M., Arndt, N. T., Barling, J., *et al.* (2000). Origin and evolution of a submarine large igneous province: the Kerguelen Plateau and Broken Ridge, southern Indian Ocean. *Earth and Planetary Science Letters* **176**, 73–89.

Frey, F. A., Weis, D., Borisova, A. Yu. & Xu, G. (2002). Involvement of continental crust in the formation of the Cretaceous Kerguelen Plateau: new perspectives from ODP Leg 120 Sites. *Journal of Petrology* **43**, 1207–1239.

Galer, S. J. G. & Goldstein, S. L. (1996). Influence of accretion on lead in the Earth. In: Basu, A. R. & Hart, S. (eds) *Earth Processes: Reading the Isotopic Code. Geophysical Monograph, American Geophysical Union* **95**, 75–98.

Gautier, I., Weis, D., Mennessier, J.-P., Vidal, P., Giret, A. & Loubet, M. (1990). Petrology and geochemistry of Kerguelen basalts (South Indian Ocean): evolution of the mantle sources from ridge to an intraplate position. *Earth and Planetary Science Letters* **100**, 59–76.

Govindaraju, K. (1989). Compilation of working values and sample description for 272 geostandards. *Geostandards Newsletter* **13**, 1–114.

Green, T. H. (1994). Experimental studies of trace-element partitioning applicable to igneous petrogenesis—Sedona 16 years later. *Chemical Geology* **117**, 1–36.

Hamelin, B., Dupré, B. & Allègre, C. J. (1986). Pb–Sr–Nd isotopic data of Indian Ocean Ridges: new evidence of large-scale mapping of mantle heterogeneities. *Earth and Planetary Science Letters* **76**, 288–298.

Hassler, D. R. & Shimizu, N. (1998). Osmium isotopic evidence for ancient subcontinental lithospheric mantle beneath the Kerguelen Islands, Southern Indian Ocean. *Science* **280**, 418–421.

Hofmann, A. W. & White, W. M. (1983). Ba, Rb, and Cs in the Earth's mantle. *Zeitschrift für Naturforschung* **38a**, 256–266.

Ingle, S., Weis, D. & Frey, F. A. (2002*a*). Indian continental crust recovered from Elan Bank, Kerguelen Plateau (ODP Leg 183, Site 1137). *Journal of Petrology* **43**, 1241–1257.

Ingle, S., Weis, D., Scoates, J. S. & Frey, F. A. (2002*b*). Relationship between the early Kerguelen plume and continental flood basalts of the paleo-Eastern Gondwanan margins. *Earth and Planetary Science Letters* **197**, 35–50.

Kent, R. W., Saunders, A. D., Kempton, P. D. & Ghose, N. C. (1997). Rajmahal basalts, eastern India: mantle sources and melt distributions at a volcanic rifted margin. In: Mahoney, J. & Coffin, M. F. (eds) *Large Igneous Provinces: Continental, Oceanic, and Planetary Flood Volcanism. Geophysical Monograph, American Geophysical Union* **100**, 145–182.

Kent, R. W., Pringle, M. S., Müller, R. D., Saunders, A. D. & Ghose, N. C. (2001). $^{40}Ar/^{39}Ar$ geochronology of the Rajmahal basalts, India, and their relationship to the Kerguelen Plateau. *Journal of Petrology* **43**, 1141–1153.

Macdonald, G. A. & Katsura, T. (1964). Chemical composition of Hawaiian lavas. *Journal of Petrology* **5**, 82–133.

Mahoney, J. J., Macdougall, J. D., Lugmair, G. W. & Gopalan, K. (1983). Kerguelen hotspot source for Rajmahal Traps and Ninetyeast Ridge? *Nature* **303**, 385–389.

Mahoney, J. J., Jones, W. B., Frey, F. A., Salters, V. J. M., Pyle, D. G. & Davies, H. L. (1995). Geochemical characteristics of lavas from Broken Ridge, the Naturaliste Plateau and southernmost Kerguelen Plateau: Cretaceous plateau volcanism in the southeast Indian Ocean. *Chemical Geology* **120**, 315–345.

Mahoney, J. J., White, W. M., Upton, B. G. J., Neal, C. R. & Scrutton, R. A. (1996). Beyond EM-1: lavas from Afanasy-Nikitin Rise and the Crozet Archipelago, Indian Ocean. *Geology* **24**, 615–618.

Mahoney, J. J., Frei, R., Tejada, M. L. G., Mo, X. X., Leat, P. T. & Nägler, T. F. (1998). Tracing the Indian Ocean mantle domain through time: isotopic results from old West Indian, East Tethyan, and South Pacific seafloor. *Journal of Petrology* **39**, 1285–1306.

Mahoney, J. J., Graham, D. W., Christie, D. M., Johnson, K. T. M., Hall, L. S. & VonderHaar, D. L. (2002). Between a hotspot and a cold spot: isotopic variation in the Southeast Indian Ridge asthenosphere, 86°E–118°E. *Journal of Petrology* **43**, 1155–1176.

Mehl, K. W., Bitschene, P. R., Schminke, H.-U. & Hertogen, J. (1991). Composition, alteration and origin of the basement lavas and volcaniclastic rocks at Site 738 southern Kerguelen Plateau. In: Barron, J., Larsen B., *et al.* (eds) *Proceedings of the Ocean Drilling Program, Scientific Results*, 119. College Station, TX: Ocean Drilling Program, pp. 299–322.

Michard, A., Montigny, R. & Schlich, R. (1986). Geochemistry of the mantle below the Rodriguez triple junction and the South-East Indian Ridge. *Earth and Planetary Science Letters* **78**, 104–114.

Neal, C. R. (2001). The interior of the Moon: the presence of garnet in the primitive, deep lunar mantle. *Journal of Geophysical Research* **106**, 27865–27885.

Neal, C. R. & Taylor, L. A. (1989). Negative Ce anomaly in a peridotite xenolith from Malaita, Solomon Islands: evidence for crustal recycling into the mantle or mantle metasomatism? *Geochimica et Cosmochimica Acta* **53**, 1035–1040.

Nicolaysen, K., Bowring, S., Frey, F., Weis, D., Ingle, S., Pringle, M. S., Coffin, M. F. & the Leg 183 Shipboard Scientific Party (2001). Provenance of Proterozoic garnet–biotite gneiss recovered from Elan Bank, Kerguelen Plateau, southern Indian Ocean. *Geology*, **29**, 235–238.

O'Hara, M. J. & Matthews, R. E. (1981). Geochemical evolution in an advancing, periodically replenished, periodically tapped, continuously fractionating magma chamber. *Journal of the Geological Society, London* **138**, 237–277.

Operto, S. & Charvis, P. (1995). Kerguelen Plateau: a volcanic passive margin fragment? *Geology* **23**, 137–140.

Operto, S. & Charvis, P. (1996). Deep structure of the southern Kerguelen Plateau (southern Indian Ocean) from ocean bottom seismometer wide-angle seismic data. *Journal of Geophysical Research* **101**, 25077–25103.

Peng, Z. X., Mahoney, J. J., Hooper, P., Harris, C. & Beane, J. (1994). A role for lower continental crust in flood basalt genesis? Isotopic and incompatible element study of the lower six formations of the western Deccan Traps. *Geochimica et Cosmochimica Acta* **58**, 267–288.

Pringle, M. S. & Duncan, R. A. (2000). Basement ages from the southern and central Kerguelen Plateau: initial products of the Kerguelen large igneous province. *EOS Transactions, American Geophysical Union* **81**, S424.

Recq, M., Brefort, D., Malod, J. & Veinante, J.-L. (1990). The Kerguelen Isles (southern Indian Ocean): new results on deep structure from refraction profiles. *Tectonophysics* **182**, 227–248.

Recq, M., Le Roy, L., Goslin, J., Charvis, P. & Brefort, D. (1994). Structure profonde du Mont Ross d'après la refraction sismique (îles Kerguelen, ocean Indien austral). *Canadian Journal of Earth Sciences* **31**, 1806–1821.

Rhodes, J. M. (1996). Geochemical stratigraphy of lava flows sampled by the Hawaii Scientific Drilling Project. *Journal of Geophysical Research* **101**, 11729–11746.

Rollinson, H. (1993). *Using Geochemical Data: Evaluation, Presentation, Interpretation*. Harlow, UK: Longman, 352 pp.

Rudnick, R. L. & Fountain, D. M. (1995). Nature and composition of the continental crust: a lower crustal perspective. *Reviews of Geophysics* **33**, 267–309.

Salters, V. & White, W. M. (1998). Hf isotope constraints on mantle evolution. *Chemical Geology* **145**, 447–460.

Salters, V. J. M., Storey, M., Sevigny, J. H. & Whitechurch, H. (1992). Trace element and isotopic characteristics of Kerguelen–Heard Plateau basalts. In: Wise, S. W., Schlich, R., *et al.* (eds) *Proceedings of the Ocean Drilling Program, Scientific Results*, 120. College Station, TX: Ocean Drilling Program, pp. 55–62.

Saunders, A. D., Storey, M., Gibson, I. L., Leat, P., Hergt, J. & Thompson, R. N. (1991). Chemical and isotopic constraints on the origin of the basalts from the Ninetyeast Ridge, Indian Ocean: results from DSDP Legs 22 and 26 and ODP Leg 121. In: Weissel, J., Peirce, J., Taylor, E. & Alt, J. (eds) *Proceedings of the Ocean Drilling Program, Scientific Results*, 121. College Station, TX: Ocean Drilling Program, pp. 559–590.

Schaming, M. & Rotstein, Y. (1990). Basement reflectors in the Kerguelen Plateau, south Indian Ocean: indications for the structure and early history of the plateau. *Geological Society of America Bulletin* **102**, 580–592.

Schlich, R., Wise, S. W., Jr, *et al.* (eds) (1989). *Proceedings of the Ocean Drilling Program, Initial Reports*, 120. College Station, TX: Ocean Drilling Program.

Storey, M., Saunders, A. D., Tarney, J., Leat, P. T., Thirlwall, M. F., Thompson, R. N., Menzies, M. A. & Marriner, G. F. (1988). Geochemical evidence for plume–mantle interactions beneath Kerguelen and Heard islands, Indian Ocean. *Nature* **336**, 371–374.

Storey, M., Saunders, A. D., Tarney, J., Gibson, I. L., Norry, M. J., Thirlwall, M. F., Leat, P., Thompson, R. N. & Menzies, M. A. (1989). Contamination of Indian Ocean asthenosphere by the Kerguelen–Heard mantle plume. *Nature* **338**, 574–576.

Storey, M., Kent, R. W., Saunders, A. D., Salters, V. J., Hergt, J., Whitechurch, H., Sevigny, J. H., Thirlwall, M. F., Leat, P., Ghose, N. C. & Gifford, M. (1992). Lower Cretaceous volcanic rocks on continental margins and their relationship to the Kerguelen Plateau. In: Wise, S. W., Schlich, R., *et al.* (eds) *Proceedings of Ocean Drilling Program, Scientific Results*, 120. College Station, TX: Ocean Drilling Program, pp. 23–53.

Sun, S.-S. & McDonough, W. F. (1989). Chemical and isotopic systematics of oceanic basalts: implications for mantle composition and processes. In: Saunders, A. D. & Norry, M. J. (eds) *Magmatism in the Ocean Basins. Geological Society, London, Special Publications* **42**, 313–345.

Tikku, A. A. & Cande, S. C. (2000). On the fit of Broken Ridge and Kerguelen plateau. *Earth and Planetary Science Letters* **180**, 117–132.

Todt, W., Cliff, R. A., Hanser, A. & Hofmann, A. W. (1996). Evaluation of a $^{202}Pb + {}^{205}Pb$ double spike for high-precision lead isotopic analyses. In: Basu, A. & Hart, S. (eds) *Earth Processes: Reading the Isotopic Code. Geophysical Monograph, American Geophysical Union* **95**, 429–437.

Toplis, M. J. & Carroll, M. R. (1996). Differentiation of ferro-basaltic magmas under conditions open and closed to oxygen: implications for the Skaergaard intrusion and other natural systems. *Journal of Petrology* **37**, 837–858.

Toplis, M. J. & Carroll, M. R. (1995). An experimental study of the influence of oxygen fugacity on Fe–Ti oxide stability, phase relations, and mineral–melt equilibria in ferro-basaltic systems. *Journal of Petrology* **36**, 1137–1170.

Weaver, B. L. & Tarney, J. (1984). Empirical approach to estimating the composition of continental crust. *Nature* **310**, 575–577.

Wedepohl, K. H. (1995). The composition of the continental crust. *Geochimica et Cosmochimica Acta* **59**, 1217–1232.

Weis, D., Bassias, Y., Gautier, I. & Mennessier, J.-P. (1989). Dupal anomaly in existence 115 Ma ago: evidence from isotopic study of the Kerguelen Plateau (South Indian Ocean). *Geochimica et Cosmochimica Acta* **53**, 2125–2131.

Weis, D., Frey, F. A., Saunders, A. & Gibson, I. (1991). Ninetyeast Ridge (Indian Ocean): a 5000 km record of a DUPAL mantle plume. *Geology* **19**, 99–102.

Weis, D., Frey, F. A., Leyrit, H. & Gautier, I. (1993). Kerguelen Archipelago revisited: geochemical and isotopic study of the Southeast Province lavas. *Earth and Planetary Science Letters* **118**, 101–119.

Weis, D., Frey, F. A., Giret, A. & Cantagrel, J.-M. (1998). Geochemical characteristics of the youngest volcano (Mount Ross) in the Kerguelen Archipelago: inferences for magma flux, lithosphere assimilation and composition of the Kerguelen plume. *Journal of Petrology* **39**, 973–994.

Weis, D., Ingle, S., Damasceno, D., Frey, F. A., Nicolaysen, K., Barling, J. & the Leg 183 Scientific Party (2001). Origin of continental components in Indian Ocean basalts: evidence from Elan Bank (Kerguelen Plateau, ODP Leg 183, Site 1137). *Geology* **29**, 147–150.

Yang, H.-J., Frey, F. A., Weis, D., Giret, A., Pyle, D. & Michon, G. (1998). Petrogenesis of the flood basalts forming the northern Kerguelen Archipelago: implications for the Kerguelen plume. *Journal of Petrology* **39**, 711–748.